ANL-77-48

PHYSICS OF REACTOR SAFETY

Quarterly Report

January—March 1977

ARGONNE NATIONAL LABORATORY, ARGONNE, ILLINOIS

Prepared for the U. S. NUCLEAR REGULATORY COMMISSION
under Contract W-31-109-Eng-38

Printed in the United States of America
Available from
National Technical Information Service
U. S. Department of Commerce
5285 Port Royal Road
Springfield, Virginia 22161
Price: Printed Copy $4.50; Microfiche $3.00

Distribution Category:
Advanced Reactor Safety
Research—Fast Reactors
(NRC-7)

ANL-77-48

ARGONNE NATIONAL LABORATORY
9700 South Cass Avenue
Argonne, Illinois 60439

PHYSICS OF REACTOR SAFETY

Quarterly Report
January—March 1977

Applied Physics Division

June 1977

Work performed for the
Division of Reactor Safety Research
U. S. Nuclear Regulatory Commission

Previous reports in this series

ANL-76-72	January—March 1976
ANL-76-114	April—June 1976
ANL-77-9	July—September 1976
ANL-77-22	October—December 1976

TABLE OF CONTENTS

TABLE OF CONTENTS

LIST OF FIGURES

LIST OF TABLES

PHYSICS OF REACTOR SAFETY

Quarterly Report
January-March 1977

ABSTRACT

This quarterly progress report summarizes work done in Argonne National Laboratory's Applied Physics Division and Components Technology Division for the Division of Reactor Safety Research of the U. S. Nuclear Regulatory Commission Applied Physics Division includes reports on reactor safety program by members of the Reactor Safety Appraisals Group Monte Carlo analysis of safety-related critical assembly experiments by members of the Theoretical Fast Reactor Physics Group, and planning of DEMI safety-related critical experiments by members of the Zero Power Reactor (ZPR) Planning and Experiments Group. Work on reactor core thermal-hydraulic performed in the Components Technology Division is also included in this report.

I. TECHNICAL COORDINATION - FAST REACTOR SAFETY ANALYSIS (A2015)

A. Summary

ENDF/B Version IV cross section were found to give an inner core sodium void worth for the CRBR at BOL 12.6% more positive than that obtained with Version III cross sections; use of transport theory in the resonance region instead of the narrow resonance approximation gave a result 7% more positive.

Coding of a pool reactor primary loop routine, PLOOP, has been completed and the code debugged.

Treatments in EPIC of interaction between newly ejected fuel particles and those already in the channel has been improved, and a more precise treatment of sodium reentry provided. Comparison between EPIC and PLUTO1 is nearly complete. Agreement is fairly good except that EPIC predicts about a 20% larger rate of fuel ejection and large upper sodium slug ejection velocities because of improved numerical techniques.

Scoping studies have been performed of recriticality caused by pressurization of part of the top area of a boiling homogenized fuel/steel pool assumed to be at prompt critical at the time pressure is applied. The pressure, 3 or 5 atm, was assumed applied either on disks of varying size or on annular rings. The initial results indicate that the pressurization must cover more than 25% of the pool area to cause a reactivity increase.

Studies of the reactivity effect of change in neutron streaming resulting from bubble collapse in a boiling fuel-steel pool (Behrens effect) have indicated that this reactivity effect is strongly dependent on whether collapse of the pool, as the result of pressure applied to the top occurs uniformly over pool volume or is localized at the top of the pool, as it is actually calculated to be. The effect is much larger in the latter case. However, there is a serious question in this case of the validity of the Monte Carlo calculation of the streaming effect on leakage, which is based on a uniform lattice of bubbles.

It has been found acceptable to remove the iteration between hydrodynamics and neutronics at the reactivity step level in FX2-POOL, thereby cutting the hydro/thermo storage in half and significantly reducing the running time of the code. It has also been found that extrapolating reactivity and other point kinetics parameters as a function of time is much more effective than extrapolating fluxes at each grid point and using those to determine the point kinetics parameters in dealing with the rapid material motions occurring when a boiling fuel-steel pool is compressed. The accuracy of the result is not affected by this simplification in extrapolation technique, which also makes possible a considerable reduction in computing time.

In order to evaluate the importance of vapor-liquid slip in boiling fuel/steel pools we have written TWOPOOL, a new two field, two phase, two dimensional Eulerian hydrodynamics routine for FX2-POOL. We have chosen to write

a new code rather than modify KACHINA, since KACHINA is based on the ICE technique which was originally designed to deal with a non-condensible gas that was not in thermal equilibrium and did not exchange mass with the liquid phase. We have considered it to be simpler and closer to physical reality to assume continual thermal equilibrium (saturation conditions) between liquid and vapor phases. Comparisons of TWOPOOL and KACHINA, both modified to make a consistent comparison possible, are now underway. Results so far indicate good agreement between the modified version of the codes except that the differencing scheme used in KACHINA appears to cause errors in the vapor velocity (for the test case) in the vicinity of the calculational boundary. These errors become smaller with grid size indicating that the source is truncation error. When reasonably sized momentum tranfer contributions due to vaporization and condensation were included, this error was no longer detectable.

B. Study of Basic Problems in Accident Analysis

1. Initiating Conditions Variations

a. Effect of Using Version-IV Cross Sections on the Sodium-Void Worth of the LWR-Pu-Fueled CRBR at BOL. (Kalimullah) The effect of using ENDF/B Version-IV cross sections on the sodium-void reactivity of the LWR-Pu-fueled CRBR at BOL has been studied by computing the total inner core void worth by k-effective difference using three different cross section sets: our standard Version-III cross section set, Version-IV cross section Set 1 generated using the narrow resonance approximation, and Version-IV cross section Set 2 generated using the RABANL integral transport theory over the resonance energy interval. The inner core void worth based on the Version-III cross sections is 1.155% Δ , and the Version-IV cross section Sets 1 and 2 give values 12.6 and 19.7% higher than this. The inner core void worth without resonance self-shielding based on the Version-III cross sections is 0.965% Δk, and the Version-IV cross section Sets 1 and 2 give values 10.3 and 17.1% higher than this. The spatial distribution of sodium void worth based on these three cross section sets has also been computed.

The inner core sodium-void worth is most sensitive to the following microscopic cross sections: (1) ^{238}U capture, (2) ^{239}Pu capture, (3) ^{239}Pu fission, (4) ^{23}Na elastic scattering, and (5) ^{16}O elastic scattering. A comparison of the Version-IV cross section Sets 1 and 2 with respect to these microscopic cross sections shows that the increase in ^{238}U capture cross sections from 3.36 to 0.10 keV causes most of the increase in the inner core void worth. In Version-IV cross section Set 2 ^{238}U capture cross sections over this energy interval are 2 to 29% higher than those in Version-IV cross section Set 1.

2. PLOOP Computer Program (Kalimullah)

Coding of PLOOP, the pool reactor primary coolant loop program, has been completed. The code is made up of three main parts: the main driver routine, a temporary routine representative of the SAS Code as far as the intercommicating variables are concerned, and the primary circuit routine. The hydraulics and to some extent the heat transfer calculations were checked for a test case in which the pump-motor speed and the sodium mass flow rate in the loop start from zero and increase to their steady-state values when the motor is turned on at zero time, the reactor power being put always zero. Most of the data were obtained from an ANL design study.

Both the hydraulics and the heat transfer transient calculations of the program were then tested and debugged by running the above test problem to about 40 seconds of transient time, with the reactor power specified to be zero during the first second and then linearly increased to full power in the next two seconds and kept constant for the rest of the transient. The variation of mass flow rate along the length of the subassembly resulting from temperature changes was up to 2%. If the reactor power is started earlier when the flow is low, this variation could be several hundred percent, because the density variations corresponding to temperature changes produce effective instantaneous flows comparable to the inlet flow rate.

3. EPIC Development (P. A. Pizzica)

A fuel-fuel drag treatment was added to EPIC so that when fuel is ejected into a coolant channel with a large fuel volume fraction, the interaction between the newly ejected fuel particles and those already in the channel is taken into account. Heretofore, the newly ejected particles were always started at zero velocity and then accelerated by the drag from the sodium. The old and new models produce the same results until there is little sodium left to accelerate the newly ejected particles, at which time, if the fuel volume fraction is large, there should be some acceleration of the newly ejected particles due to interaction with the existing particles. At a fuel volume fraction less than 0.3, there is no effect; at a fuel volume fraction greater than 0.7, there is assumed instantaneous equilibration of velocities (with conservation of total momentum); in between 0.3 and 0.7, the velocity of the newly ejected particle varies linearly with the volume fraction of the fuel from zero up to the equilibrated velocity at 0.7 volume fraction (with conservation of momentum).

Also, a more precise treatment of sodium re-entry events was included in the code so that TOP conditions would be more accurately treated. In the old model, due to an imprecise treatment of the lower slug interface in such conditions, the mixing of fuel and sodium was incorrectly treated.

4. EPIC/PLUTO1 Comparison (P. A. Pizzica and J. J. Sienicki)

The comparison study between PLUTO1 and EPIC is almost completed and a full report will be issued in the near future. The results of a TOP case for a demonstration-size reactor are shown in Figs. 1-5. Figure 1 shows the upper sodium slug velocity for the two cases. The behavior is similar except that, due to the higher pressures that are produced in the channel in EPIC, the impulse on the slug is greater. The greater channel pressures in EPIC are mainly due to the difference in pin numerics which were explained in great detail in the January-March 1976 quarterly and in the Chicago Safety Meeting paper on EPIC.[1] For this same reason, EPIC predicts more fuel ejection than PLUTO (Fig. 2). EPIC moves fuel in the molten fuel cavity in the pin toward the cladding breach more readily than PLUTO since there is too much retardation of fuel flow in PLUTO1 because of the artificial viscosity terms in PLUTO's pin momentum equation. Since channel pressures predicted by EPIC are higher, at least initially, the lower sodium slug takes longer to re-enter in an EPIC calculation, and the re-entry FCI's are delayed some 15 msec over PLUTO1. (This is seen in the "spikes" in the PLUTO calculation temperature plot of Fig. 3. These spikes result from the fact that as the sodium in the cell containing the lower slug interface heats up the interface moves to the

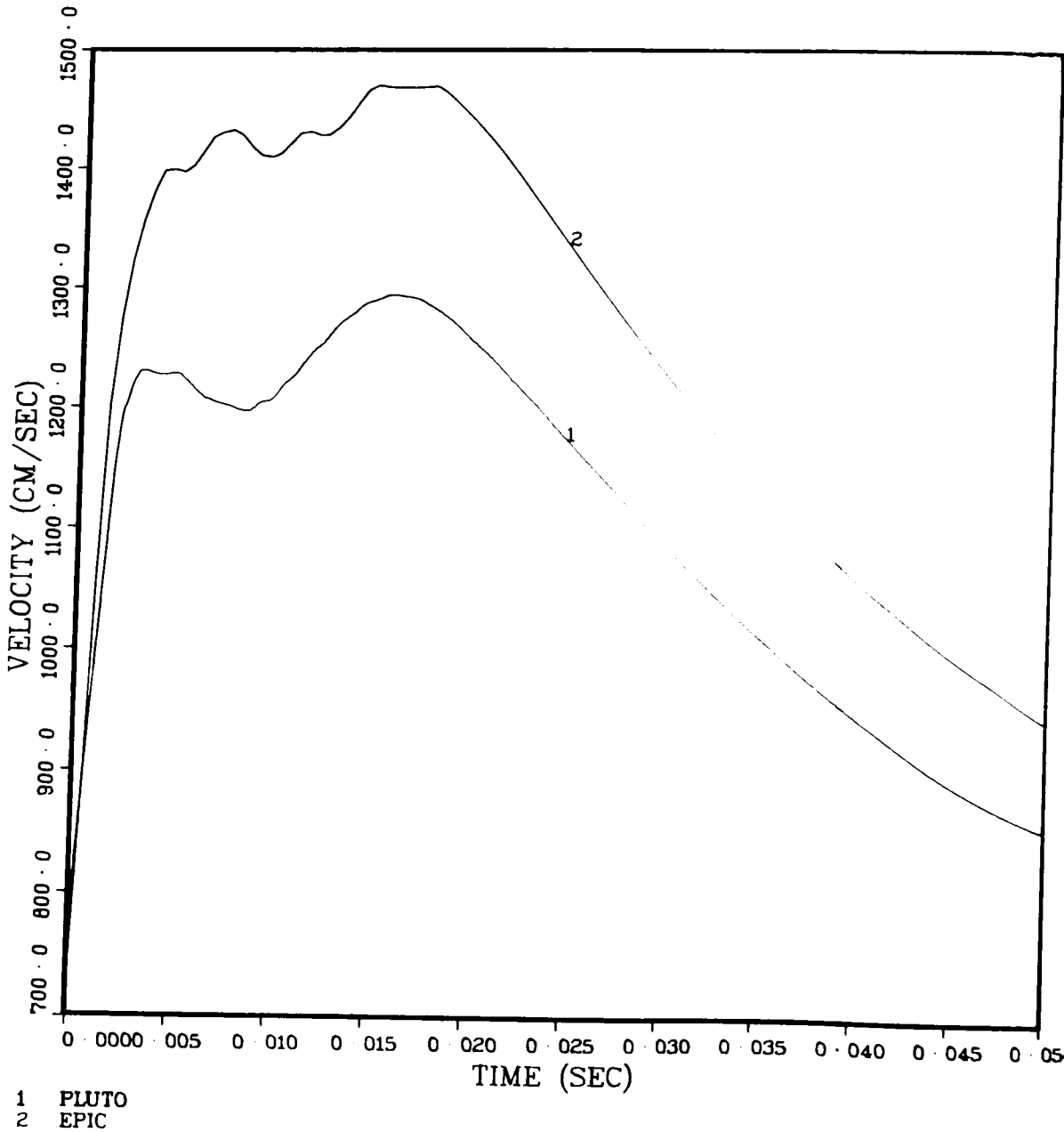

Fig. 1. Upper Slug Velocity vs. Time
ANL Neg. No. 116-77-330

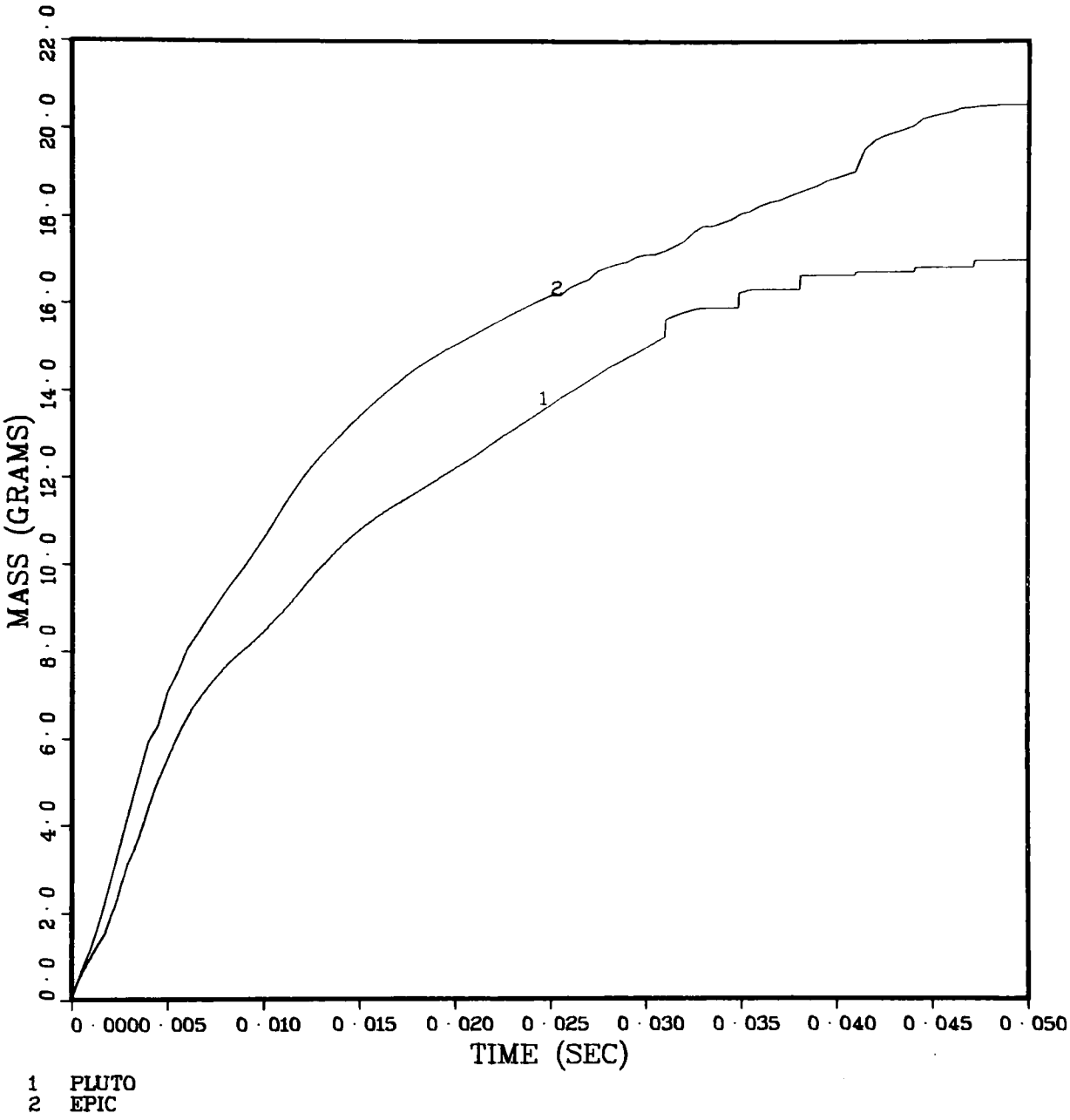

Fig. 2. Total Fuel Ejected into Coolant Channel vs. Time
ANL Neg. No. 116-77-326

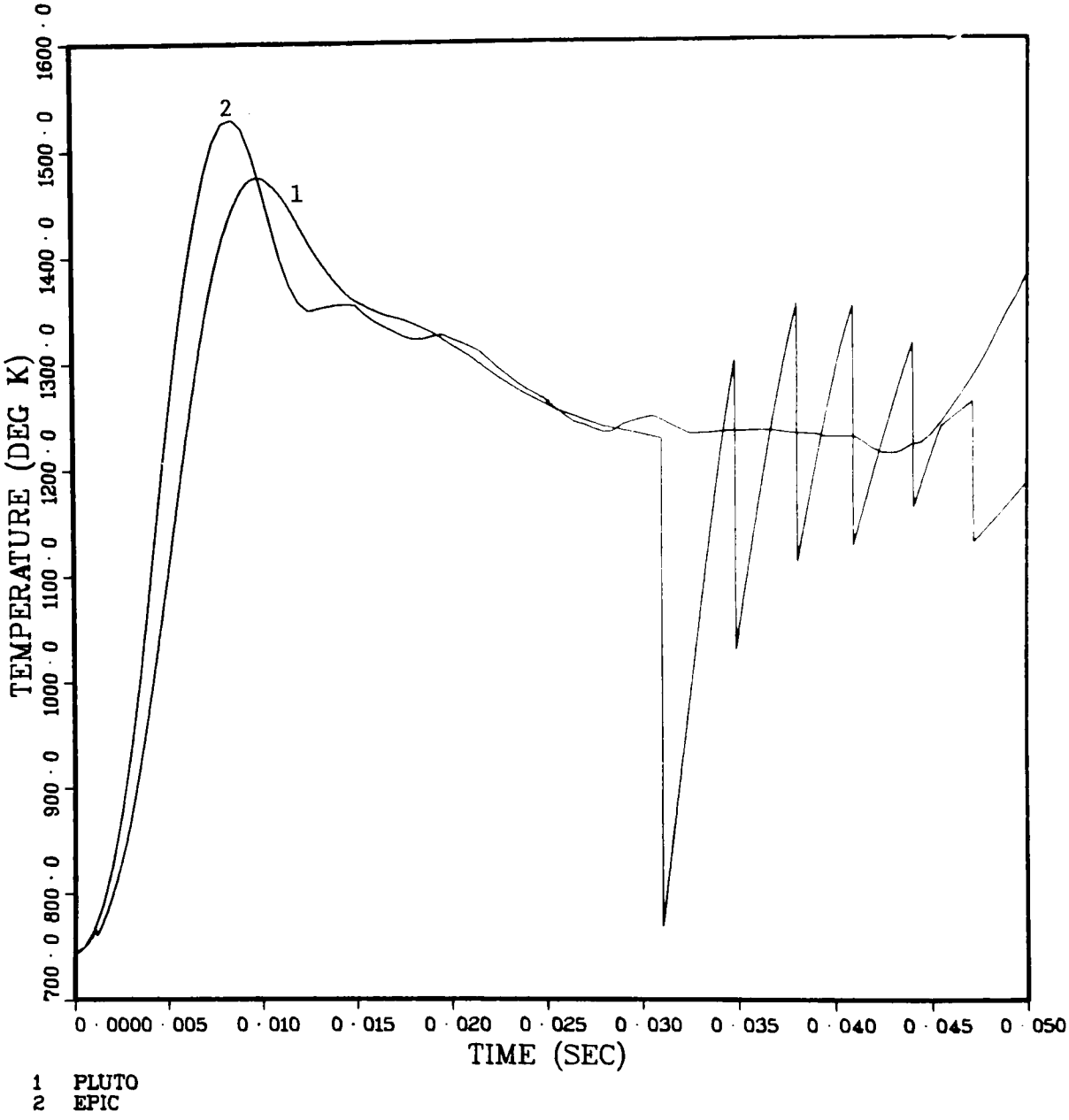

Fig. 3. Sodium Temperature at the Ejection Node vs. Time
ANL Neg. No. 116-77-328

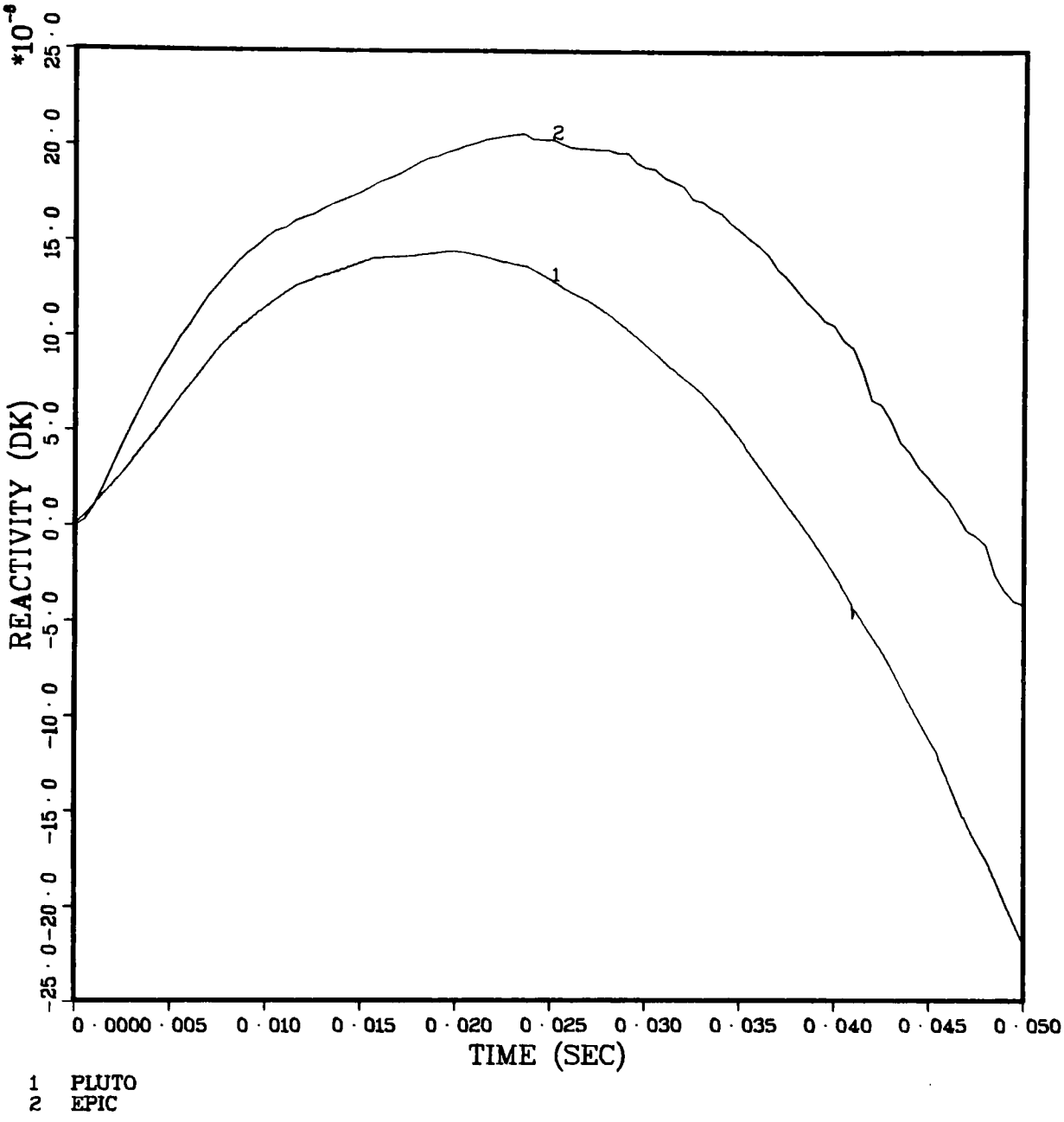

Fig. 4. Total Reactivity vs. Time
ANL Neg. No. 116-77-327

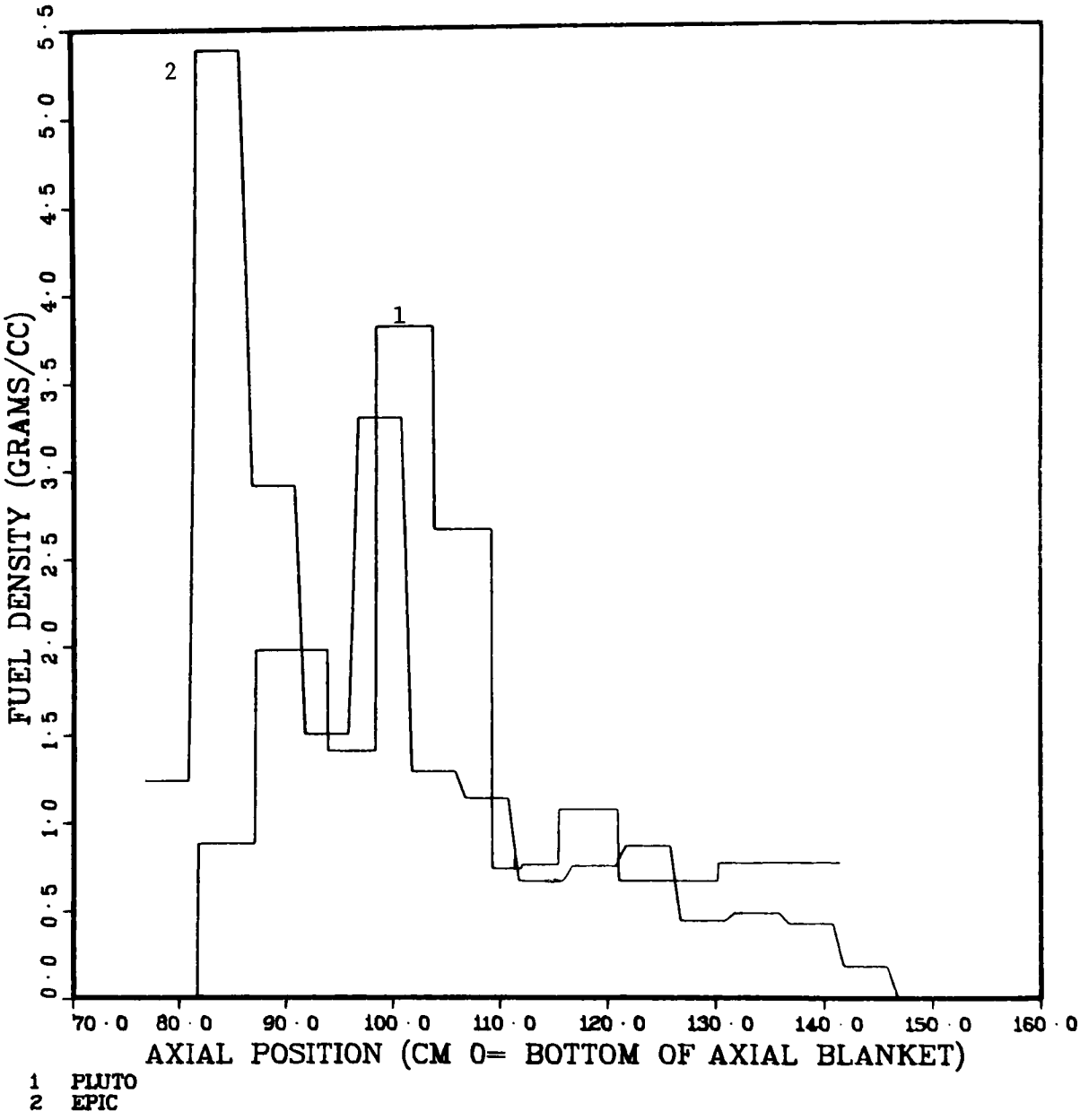

Fig. 5. Fuel Distribution in Coolant Channel at Time = 0.050 sec
ANL Neg. No. 116-77-329

next cell downward, and since it is the pressure of the interface cell that is being plotted a discontinuity develops at the time the definition of this cell changes. This is characteristic of Lagrangian numerics). Since EPIC predicts more fuel ejected into the channel than PLUTO (Fig. 2) EPIC's total reactivity curve (Fig. 4) is higher. This also explains why EPIC has more fuel in front of the rupture at 50 msec (Fig. 5) than PLUTO, since PLUTO's fuel ejection (Fig. 2) is almost entirely cut off after 35 msec because the re-entry FCI raises the channel pressure. (The reentry FCI begins in EPIC at about 47 msec).

Also included are three graphs showing the results of fuel ejection from a pin through four failure nodes into a channel that is 60% uniformly voided under LOF conditions. This is some preliminary work done for the EPIC parameter study which will be completed in the near future, at which time a full report will be issued. The parameter study will cover cases which PLUTO cannot handle such as voided coolant channels and multiple node failures Fig. 6 shows the total fuel ejected over 50 msec, Fig. 7 the total reactivity and Fig. 8 the distribution of fuel in the channel at 50 msec.

5. Recriticality in Boiling Pools (P. B. Abramson)

Scoping studies were performed of recriticalities caused by pressurization of part of the top of a boiling homogenized fuel/steel pool. The initial results indicate that the pressurization must cover more than 25% in order to cause a reactivity increase (if the pool is assumed to be initially at prompt critical).

The initial studies were carried out for a pool of 100-cm radius and 100-cm depth at roughly 40% fuel volume fraction, 40% steel volume fraction and 20% vapor, at an initial temperature of 4000°K (in thermal equilibrium). The system, which was assumed to be at prompt critical, was then subjected to a pressurization on the top surface of various magnitudes and geometrical shapes. The shapes were:

a) disk
   i.e. pressurization from r = 0 to R, where:
   $R = 0.25\ R_o,\ 0.5\ R_o,\ 0.75\ R_o$

b) ring
   i.e. pressurization from R to R + Δr where $\Delta r = 0.05\ R_o$
   and R = 0.25 R, 0.5 R or 0.75 R

Since the system was assumed to be prompt critical, the power rose in all cases. However in nearly all cases, the reactivity monotonically decreased due to geometry changes. It was only in those cases of disk shaped pressurizations with $R > 0.5\ R_o$ that the reactivity increased.

We hasten to point out that these are scoping studies and very limited in number to date and that further studies will certainly clarify the types of pressure sources necessary to cause reactivity increases under various initial conditions.

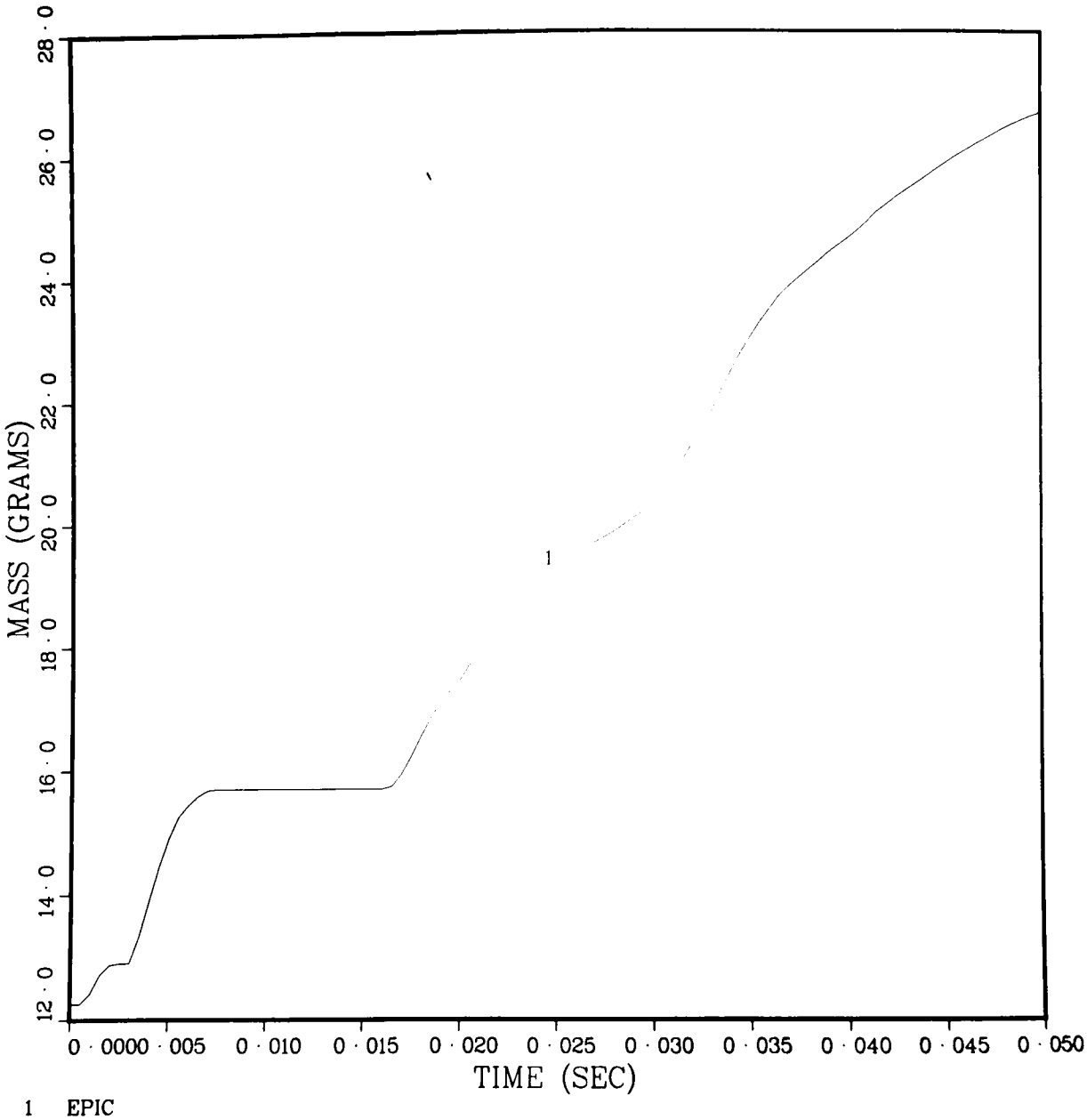

Fig. 6. Total Fuel Ejected Into Coolant Channel vs. Time
ANL Neg. No. 116-77-412

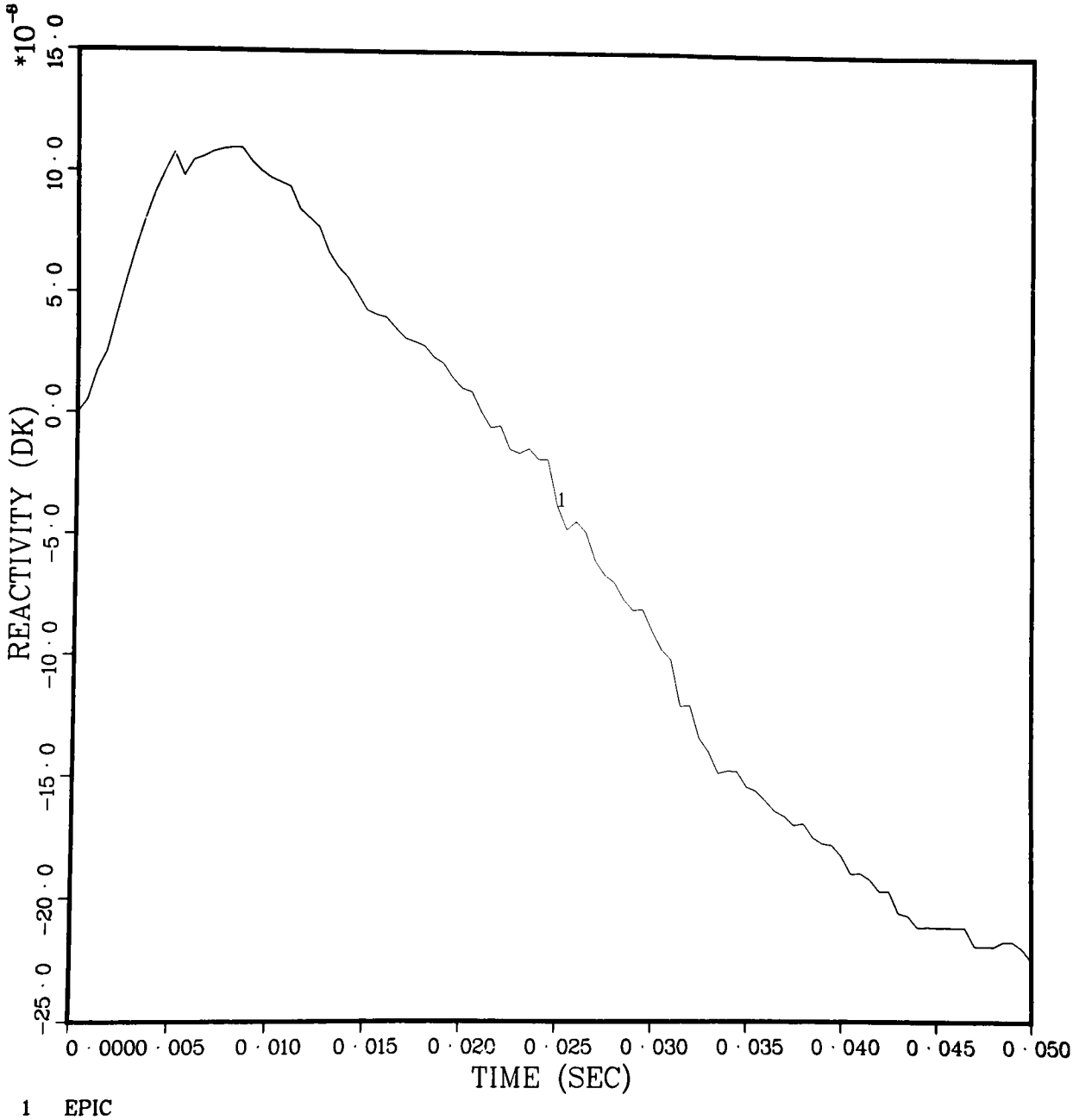

Fig. 7. Total Reactivity vs. Time
ANL Neg. No. 116-77-413

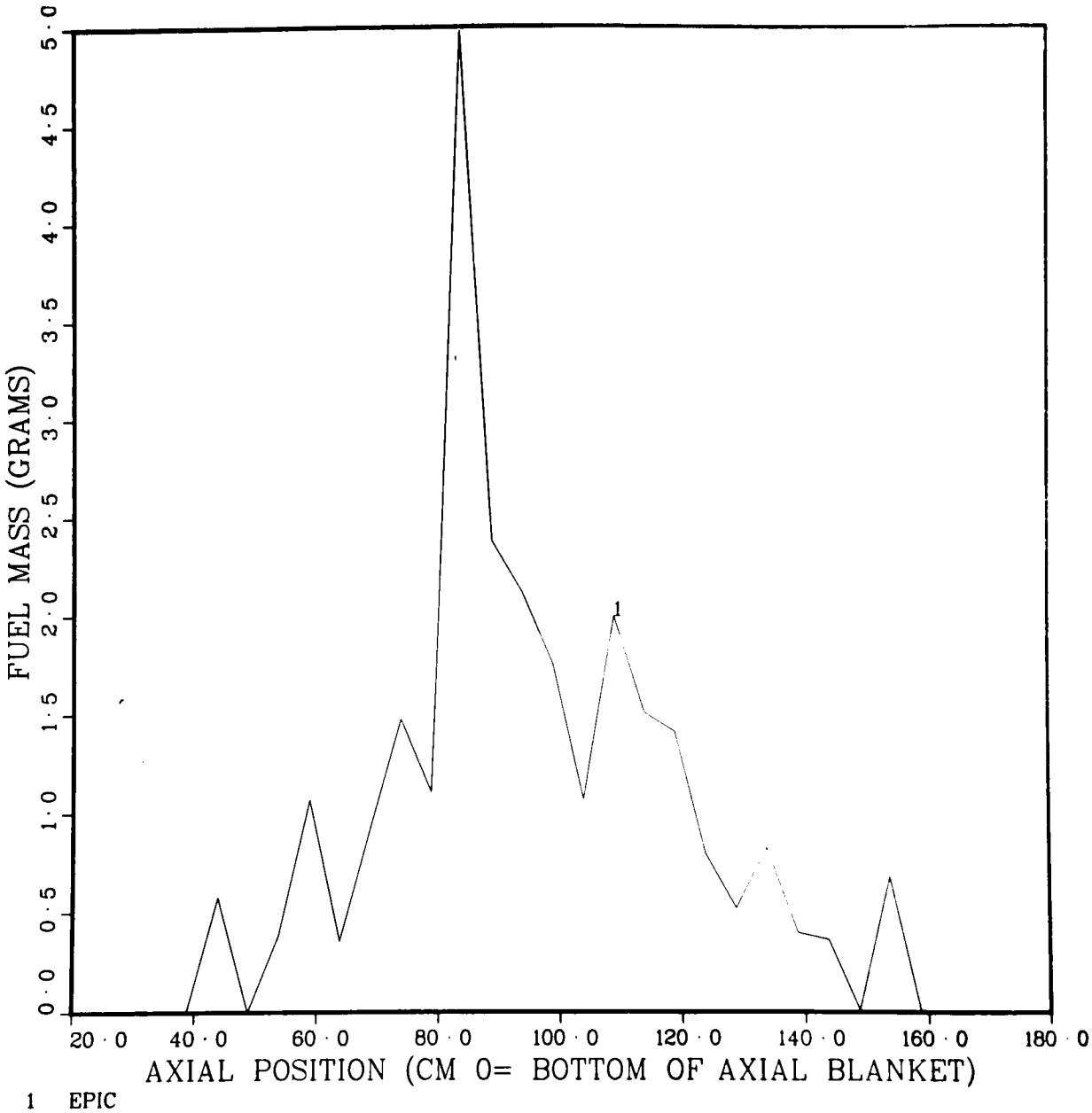

Fig. 8. Fuel Distribution in Coolant Channel at Time = 0.050 sec
ANL Neg. No. 116-77-404

Figure 9 (Pressure Pulse Effect on Accident Energetics) - shows the effect of the pressure amplitude and the disk outer radius upon the power level for these perturbations. While there is some power rise for the 3 and 5 atm (additional) top pressurization when applied to R = 0.5 R_o as compared to to R = 0.25 R_o, there was a $\Delta\rho$ of less than 1¢ in the 5 atm pressurization and $\sim$ 1/2¢ in the 3 atm pressurization. Table 1 indicates the reactivity gains and maximum temperature rises associated with these excursions.

We observe that there is very little reactivity effect for those pressurization of R $\leq$ 0.5 R_o. The temperature rise (and power rise) observed for pressurization with R $\leq$ 0.5 R_o are predominantly due to the initial reactivity of \$1.

To determine the effect of pressure amplitude with a small R, we varied the amplitude from 3 atm to 100 atm for R = 0.25 R_o. These, rather interesting, results are shown in Fig. 10 (Effect of Pressure Amplitude on Power Spike). Here we note that increasing the pressure actually causes a decrease in energy deposition. This is due to the fact that the geometrical motions drive the pool into a less reactive configuration - (and was carefully checked with static "k" calculations). Thus, larger pressures drive the pool into this less reactive configuration more rapidly - hence the results of Fig. 10.

An additional example of this phemonemon is found in the examination of reactivity vs. time when the pool is subjected to a ring shaped pulse of Δr = 0.05 R_o. Figure 11 (Pulse Variation Effect on Reactivity) shows these results. We observe the following consistency in the results: higher pressurizations cause the reactivity to drop more sharply. Finally, we observe that the pulse applied at R = 3/4 R_o has a less negative reactivity effect than those at 1/2 R_o or 1/4 R_o.

All the above results are very sensitive to the hydrodynamic modeling and we expect the results to be different when studied with TWOPOOL, since vapor/liquid slip can play a very important role in these investigations.

Finally, we point the reader to our section on the Behrens effect since none of the above studies included that effect and it is in this sort of problem where this effect is paramount.

6. Behrens Effect Studies (P. Abramson, T. Daly, R. Lell and E. Gelbard)

In our studies of boiling pool recriticalities, one of the phenomena which appears to be important is the the addition of reactivity due to reduction in neutron streaming. This effect can add reactivity at two stages in the recriticalities we are examining. First, since we are looking at surface pressurizations and the concomitant surface compactions, there is a reduction in streaming at the surface and an accompanying reactivity increase that would not be accounted for in an ordinary diffusion theory calculation. Second, if the system becomes super prompt critical (which last only a few milliseconds) the neutronic energy causes the liquid fuel to heat up and causes the liquid phase to expand into the space initially occupied only by vapor. This short-time swelling and concurrent reduction of relative vapor volume takes place at constant local smeared density and causes the system to proceed from a non-homogenized toward a homogenized system, and this causes the system to progress toward a less leaky configuration and adds reactivity. McLachlan[2] has

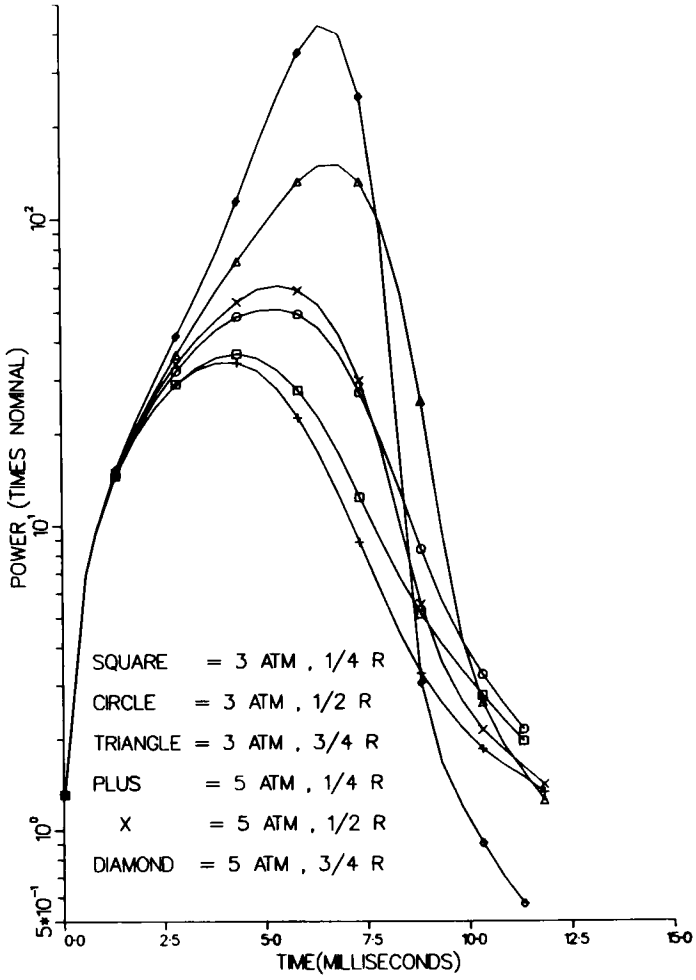

Fig. 9. Pressure Pulse Effect on Accident Energetics
ANL Neg. No. 116-77-70

TABLE I. Reactivity and Temperature Rises for Disk Pressurization

Disk Outer Radius	Pressurization, atm	ρ max, ¢	ΔT Final, °K
0.25 R_o	3	0.00	150
0.25 R_o	5	0.02	136
0.5 R_o	3	0.51	217
0.5 R_o	5	0.99	234
0.75 R_o	3	2.56	488
0.75 R_o	5	6.95	911

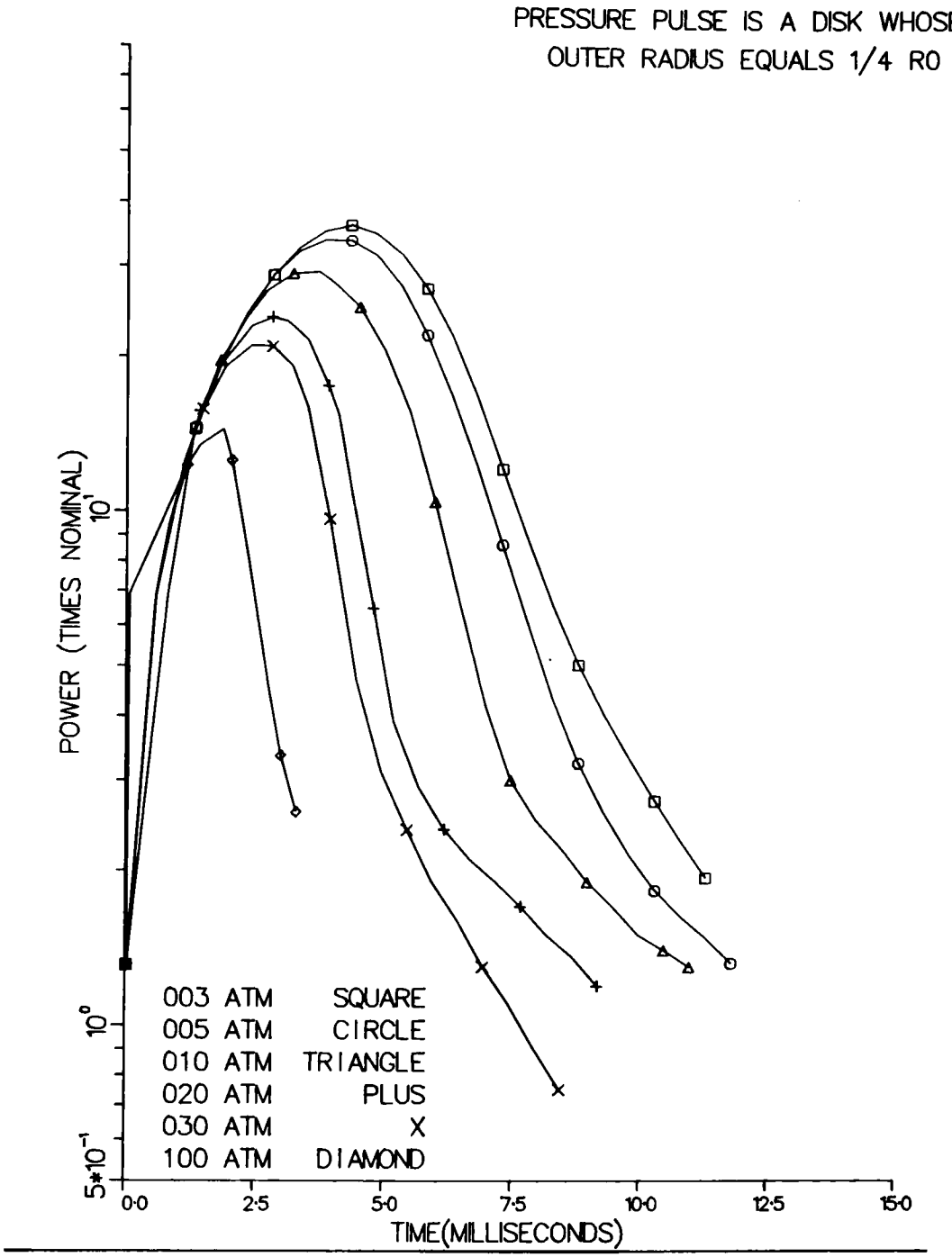

Fig. 10. Effect of Pressure Amplitude on Power Spike
ANL Neg. No. 116-77-154

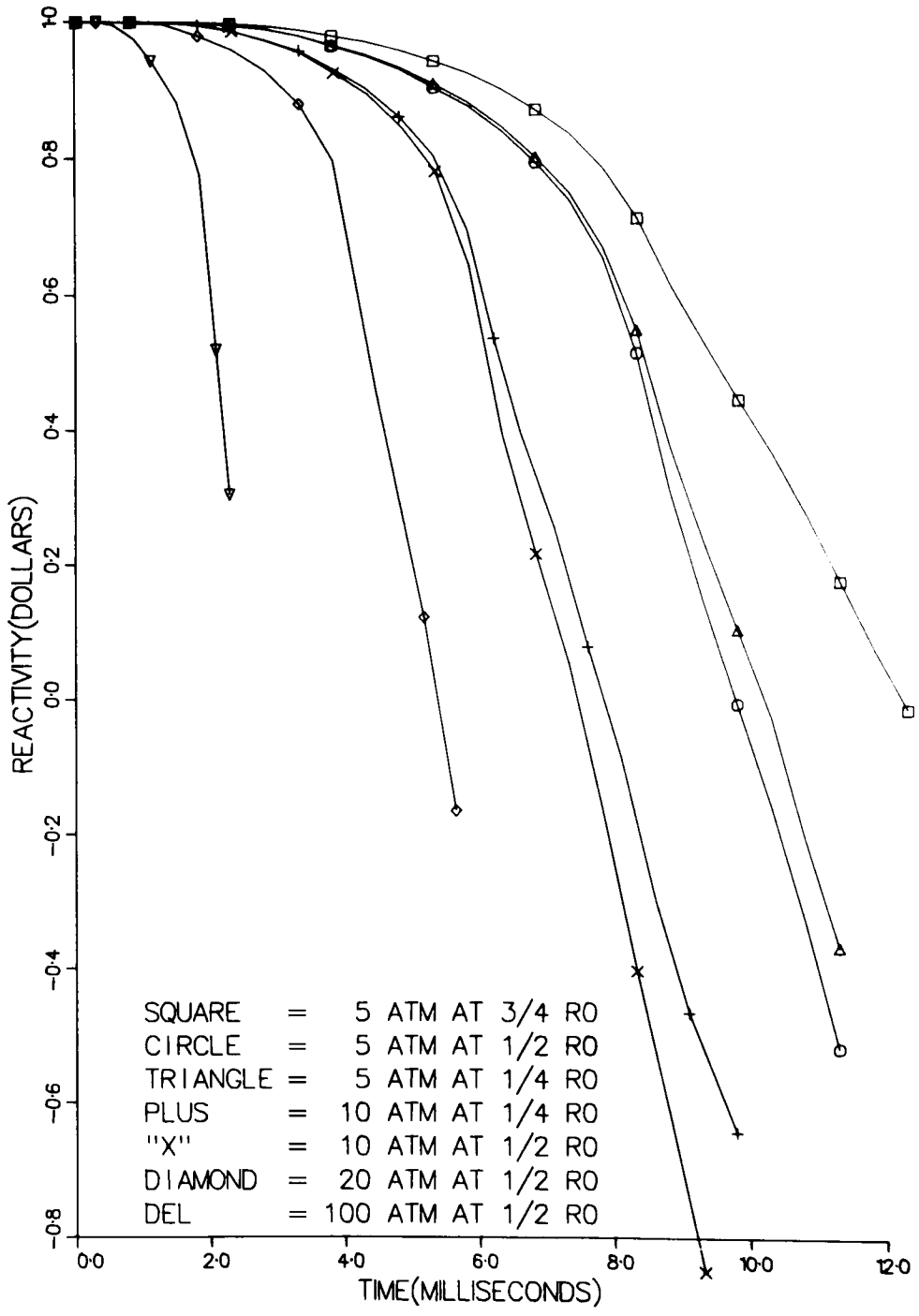

Fig. 11. Pulse Variation Effect on Reactivity
ANL Neg. No. 116-77-298

studied this effect using an S_n code and a model which has concentric spherical shells of alternating liquid and vapor. A disadvantage of this one-dimensional concentric shell model is that thermal expansion of a shell causes it to increase its average radius while expansion of a region containing bubbles immersed in a liquid would merely compact the bubbles. Nicholson[3] and Fuller[4] have examined the effect for HCDA's using VENUS[5] and the Behrens formula.[6]

Our models describe a boiling pool of fuel and steel (in the transition phase) containing a semi-random distribution of bubbles and employing recent[7,8] Monte Carlo calculations for bubble distributions. We have applied the Monte Carlo results in an RZ diffusion theory calculation with FX2-POOL[9] to calculate the additional energy deposition due to bubble collapse effects. Our numerical approach has been to modify FX2 to correct the transport cross sections in each group in each mesh cell by a correction computed from results from the Monte Carlo calculations described in references 7 & 8. These corrections account for the increase in neutron leakage as a function of local vapor fraction and bubble radius.

For situations wherein the entire pool is uniformly compressed, we find that the reactivity gain in the non homogenized system (for bubbles on the order of 1 cm and vapor fractions on the order of 30%) is between 1.5 and 2.0 times the corresponding reactivity increase in a bubble free homogeneous system. This is consistent with our results obtained using the Behrens formula and consistent with those results of references 3 & 4. However, for boiling pools with a surface pressure (i.e. a pressure applied uniformly to the top) we find that the Behrens effect can cause as much as an order of magnitude increase in reactivity ramp.

Figure 12 show the influence of the bubble collapse on the power of a pool (described in our section on recriticality) to a uniform pressure of 3 atm applied to the entire top surface. The homogenized calculation did not include the bubble collapse effect while the curve labeled "bubbly pool" did include this effect. Two phenomena are present. First, and predominating in this case, is the surface compression effect. This compression takes place singularly near the pool top edge and is thus particularly effective in diminishing leakage.[10] Second, is the autocatalytic effect that once the power is high, the liquid phase thermal expansion in the pool center (where the power peaks) tends to further reduce the streaming.[10] In our calculations it is very difficult to separate these phenomena, but we have checked the initial Δk's due to the surface compression by comparing static k calculations with and without the Behrens effect and have obtained excellent agreement with the dynamic FX2-POOL calculations.

For example, if the top 5-cm layer of a 100-cm deep pool (of 100-cm radius) is compressed to 2 1/2 centimeters while the remainder of the pool is uncompressed, the Δk for a homogeneous calculation is 2 cents while the Δk in a bubbly calculation is 17 cents. However if that same 100-cm pool is uniformly compressed to 97.5-cm depth the Δk for a homogenous calculation is still on the order of 2 cents while the Δk for the bubbly pool is only on the order of 3.5 cents. This points out that the effect is predominant only for surface compression and confirms the intuitive impression one might have that, if leakage effects are important anywhere, it would be at the edge.

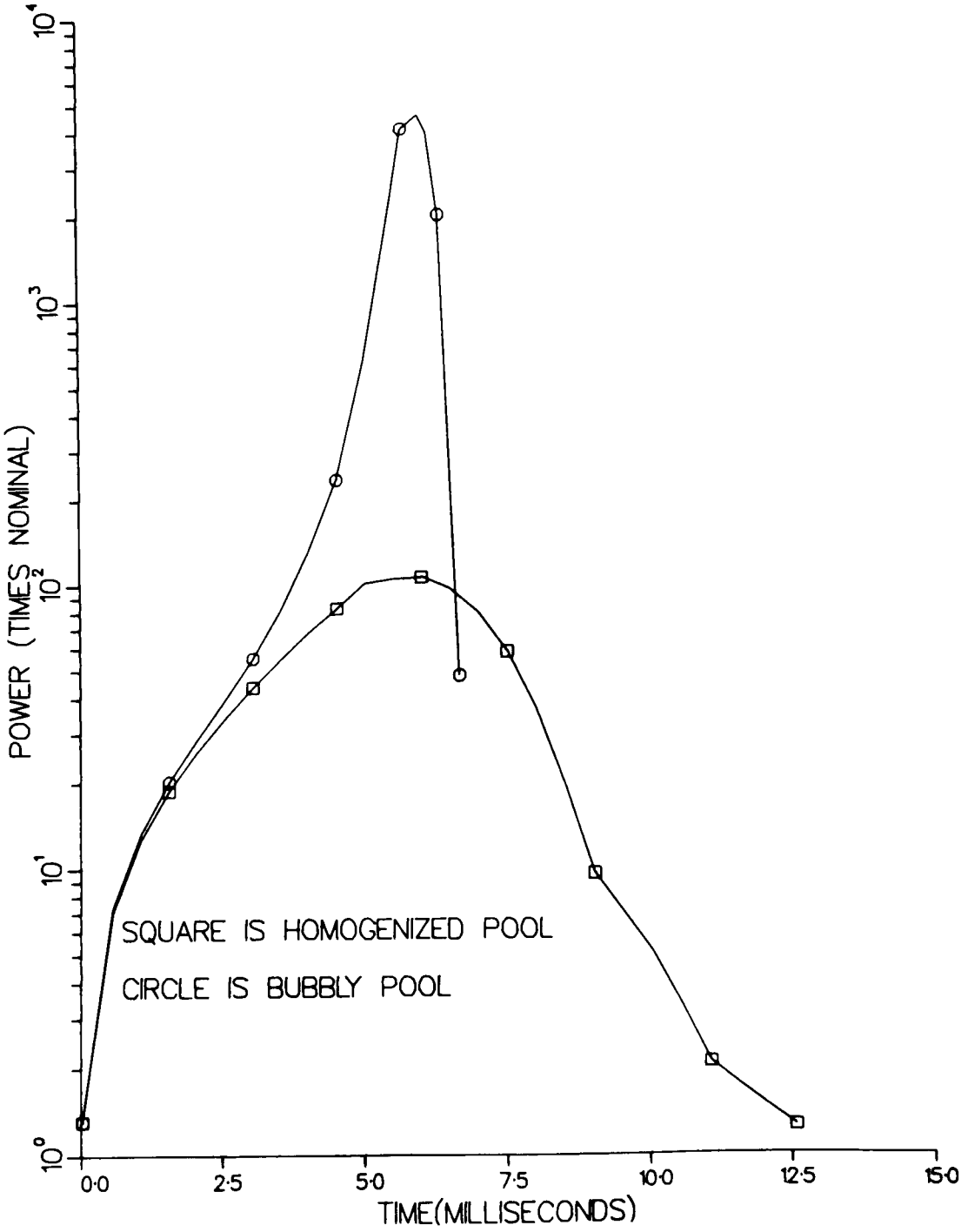

Fig. 12. Bubble Effect on Prompt Burst Power
ANL Neg. No. 116-77-147

This raises the major question, however, of the validity of our calculational method which assumes an infinite lattice of bubbles. While such an assumption may at best be valid near the center of the pool (if the bubble size and distribution isn't varying rapidly with space) it is very questionable near the edge where steep vapor fraction gradients are present. In all published work to date on the Behrens effect, this assumption has been made.

It is our intent, if funding permits, to pursue this issue, since it is apparent that the vapor fraction collapse effect is important in the study of recriticalities. Finally, of course, we must point out that the hydrodynamic modeling is paramount in this issue. If the system is foam-like, a no vapor/liquid slip model might be very good (as it might also be if it is a weakly dispersed system), but if the system is highly dispersed, vapor will slip by the liquid as the vapor attempts to pressurize the surface and the compression will not be nearly as strong or as localized as we have predicted with POOL. This phonomenon will also be investigated with FX2-TWOPOOL (described in another section of this report).

7. FX2-POOL Development - New Explicit FX2 Neutronics Calculation
(T. A. Daly & P. B. Abramson)

We have made two major changes in the iteration schemes in FX2-POOL, both improve the speed/size of the calculation and neither appears to significantly affect accuracy.

First, we have removed the iteration between hydrodynamics and neutronics at the reactivity step level as unnecessary.

The reasons for this are twofold:

1. If the reactor is on a prompt burst, such small time steps are required for the neutronics portion of the calculation that there is very little hydrodynamic or thermodynamic state change during that time step (and it can be controlled by the time-step selection criteria in FX2 and accounted for by proper time differencing in the thermodynamics).

2. If the reactor is not on a prompt burst, the power is changing quite slowly and one can do simple and very adequate time average estimates of neutronic variables for use in the thermal-hydraulics section.

By removing this iteration, we are able to reduce the hydro/thermo storage in half and significantly reduce the running time.

The second change is in the reactivity extrapolation technique used in the reactivity steps which are normally done as substeps (in between the shape steps) in the space-time kinetics.

The solution technique used by FX2 belongs to a class of methods in which the total flux is factored into a purely time-dependent function (amplitude) and a space-energy-time dependent function. The former function may vary rapidly while the latter varies slowly. As a result of this factorization, FX2 was designed to iterate between the neutronics equations and the thermal hydraulic equations.

The space-energy-time dependent (shape) function depends mainly on changes in material positions and densities which are slow relative to the prompt neutron generation time and hence the shape function is assumed to be piecewise linear over each shape time step. This is done to estimate the integrals which are the point kinetics parameters, which are then used to solve the thermal hydraulic equations.

For the particular transient which we have been studying (a constant pressure applied across the top of a pool of molten fuel and steel, which consecutively compresses the upper layers of the pool creating a more reactive configuration, and therefore causing a continuous gradual change in the global reactivity, ρ the standard FX2 technique fails. As the fuel is compressed down from the upper layers, the linear extrapolation of the local cell by cell neutron fluxes (which are then integrated to calculate reactivity, ρ) fails, resulting in the divergence of the iteration between the hydrodynamics and the neutronics. This same divergence of the iterations can be reproduced in the FX2-VENUS II production code by simulating the transient described above (i.e. using the driving function to compress the fuel and steel into lower layers of mesh cells at the same rate as the molten-fuel problem). This problem has been encountered before[11,12] and was simply bypassed by requiring that no cell have a vapor fraction larger than 0.99. It can also be bypassed by requiring that no cell have a diffusion coefficient greater than a set limit (say 10 or 20).

However, the problem can be solved (rather than the symptoms alleviated) by substitution of a less sophisticated and more direct method of extrapolation. Since we know that the reactivity, ρ, is a continuous function of time, the solution to this problem was to use an explicit technique to estimate the point kinetics parameters. Instead of a mesh cell by mesh cell linear extrapolation of the neutron fluxes, a global history of the point kinetics parameters (reactivity, delayed neutron fraction, neutron generation time) was maintained for each solution of the neutronic equations. A "moving" quadratic function for each parameter was fitted exactly as a function of time at the last three shape function calculations, and these quadratic functions were used to predict behavior as the calculation moved out over the next shape step. The results of this procedure were validated at the end of the next shape function calculation when FX2 goes back over the reactivity steps and updates these point kinetic parameters. Since the γ-factor of the shape function converges to unity we know that we have a achieved a consistent balance between the amplitude function and the shape equation. Figure 13 shows the correction made in the given transient.

The implication of predicting reactivity, ρ, directly is that we no longer have an amplitude iteration in the calculation. Thus at each reactivity step the reactivity (and hence point kinetics) will be predicted in exactly the same fashion. Since this method of estimating reactivity is much simpler than the method used in FX2, considerable savings in computing time are available, and there are also considerable savings in the amount of data management required.

Another implication is that we are partially driving the system by predicting the reactivity. The correct convergence between the neutronics equations and the thermal-hydraulic equations confirms that a consistent set of results is being maintained.

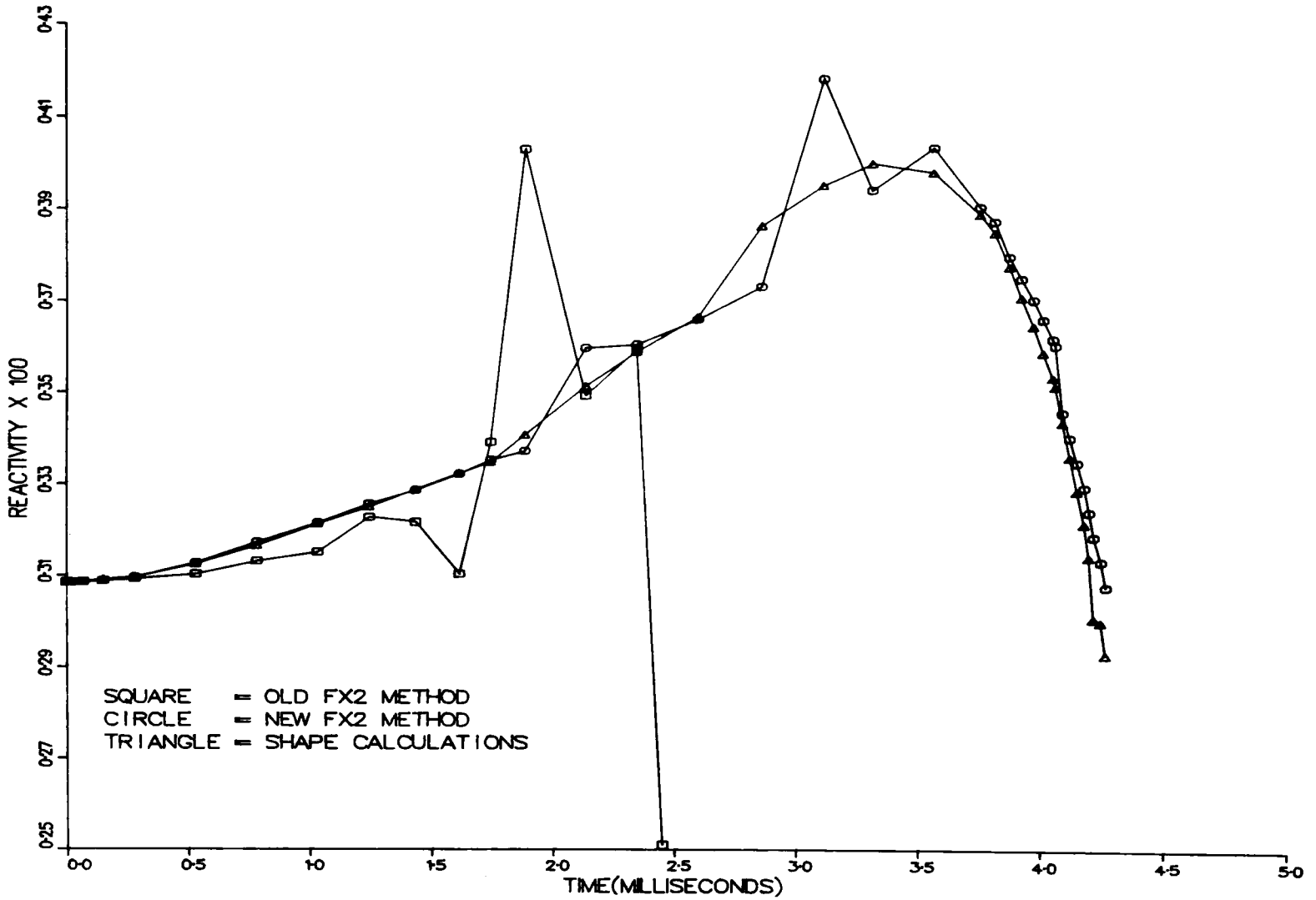

Fig. 13. Old vs. New Methods for Reactivity Extrapolation
ANL Neg. No. 116-77-153

This work will be reported at the June 1977 ANS meeting.

8. TWOPOOL Development

a. Modeling Assumptions (J. J. Sienicki & P. B. Abramson) A major assumption made in FX2-POOL is that no slip is assumed between liquid and vapor in the hydrodynamics calculation. After giving thought to the modeling of two phase flow in fuel-steel pools which can undergo high ramp rate prompt burst excursions, we have written TWOPOOL, a new two field, two phase, two dimensional Eulerian hydrodynamics routine for FX2-POOL.

The present version of TWOPOOL calculates the hydrodynamic motions of coupled liquid and vapor fields, with the basic hydrodynamic assumption that liquid fuel is assumed to exist as droplets dispersed in continuous vapor.

Particular attention has been paid to modeling the thermal interactions between a liquid, such as fuel, and its vapor, which are (as in the current version of POOL) assumed to remain in thermal equilibrium. Thus, the vapor internal energy per unit mass is assumed to equal the liquid internal energy per unit mass plus the heat of vaporization, while mass transfer between the two phases is calculated using an equilibrium thermodynamics approach.

The TWOPOOL equations for the common liquid-vapor temperature and the vapor and liquid volume fractions include effects of vaporization and condensation, the assumed rapid liquid-vapor heat transfer which maintains thermal equilibrium, convection of liquid and vapor mass and energy, compressional work performed upon the vapor, drag dissipation in the vapor, and fission heating. The separate liquid and vapor velocity fields are coupled through drag and phase change terms. The drag terms depend parametrically upon a "droplet radius" and a power of the vapor volume fractions (which is intended to account for droplet interactive effects). The driving pressure for the two coupled sets of hydrodynamic fields (vapor and liquid) is taken to be the vapor pressure of the liquid-vapor system. The pressure, liquid and vapor physical densities, liquid internal energy per unit mass, and heat of vaporization per unit mass are general temperature dependent functions.

Finite difference equations are solved for the liquid-vapor temperature, liquid and vapor volume fractions, and liquid and vapor velocities. All terms in the finite difference equations are formulated implicitly using the time centered Crank-Nicholson prescription. To achieve numerical stability, convective terms are upwind differenced. The semi-implicit method of solution used in POOL and EPIC is employed.

To follow extended motions in a high ramp rate disassembly, it is necessary to treat single phase regions. Our initial attempts to obtain a semi-implicit solution of the full single phase equations were unsuccessful; therefore, such regions are currently calculated in TWOPOOL by solving the single phase equations assuming that radial and axial motions are uncoupled. This is an area which will receive significant future attention.

The present version of TWOPOOL treats two phases of only one material, but extensions to treatment of two materials is straightforward. In the POOL/TWOPOOL formulation, steel in the pool is assumed to remain separately in

thermal equilibrium with its vapor, and this assumption of separate thermal equilibria for fuel and steel allows extension to more than one material without major difficulty.

In contrast to KACHINA, TWOPOOL does not use the pressure formulation ICE technique methods for numerical solution of its hydrodynamics equations. This is due to the that we wish to model different physics than KACHINA models. The ICE methods are designed for treatment of a two phase system in which one of the phases is a noncondensable gas which need not be in thermal equilibrium with the liquid phase. However, the standard ICE technique methods only treat only systems for which the pressure of the vapor field is weakly temperature dependent. In HCDA's the vapor pressure is dependent strongly upon the fuel temperature. KACHINA is thus oriented towards physical systems which are different from those of interest to us, and we chose to develop our own numerical modeling and techniques rather than to follow the SIMMER approach of adopting KACHINA to a different problem than that for which it was originally designed.

To check our numerical hydrodynamic techniques, we are currently comparing TWOPOOL with KACHINA. Once this comparison is complete, we will use FX2-TWOPOOL to scope the importance of such factors as liquid-vapor slip, liquid-vapor energy and mass transfer, and uncertainties in vapor density.

We also plan to review the thermal-hydraulic modeling and numerical methods in SIMMER to understand to what extent SIMMER differs from KACHINA. This will permit a more meaningful comparison between SIMMER and FX2-TWOPOOL.

b. TWOPOOL - KACHINA Comparison (J. J. Sienicki & P. B. Abramson)

In order to check the numerical techniques in TWOPOOL, comparison with KACHINA was begun and very good agreement was obtained for the example problems. Since the two codes were developed to address problems processing very different physics, direct comparison was not possible and modeling modifications to both codes were necessary to allow comparison of numerical hydrodynamic techniques.

For the comparison, we created a special version of TWOPOOL, which we call KPOOL. KPOOL and the modified KACHINA employ different finite difference formulations of equivalent continuum equations which are written in different forms. Results obtained with the two codes therefore differ slightly due to different truncation error terms. The code calculated differences have been shown to decrease as the mesh cell widths decrease and therefore differ slightly due to due to spatial truncation error effects. To better understand these truncation error effects, another version of TWOPOOL which we call KPOOL1, was written. KPOOL1 employs a differencing scheme similar to that used in KACHINA. KPOOL1 and the modified KACHINA agree nearly exactly for all cases run.

The comparison problems which we have solved are related to following extended motions in a hypothetical high ramp fast reactor disassembly following neutronic shutdown. Figures 14-17 show results typical of those obtained throughout the comparison. For this axial one dimensional problem, KPOOL, the modified KACHINA, and KPOOL1 are given zero initial velocities, an initial vapor volume fraction of 0.3, and an initial temperature profile which varies axially from 5500 K to 1800 K as a cosine across a cylindrical reactor

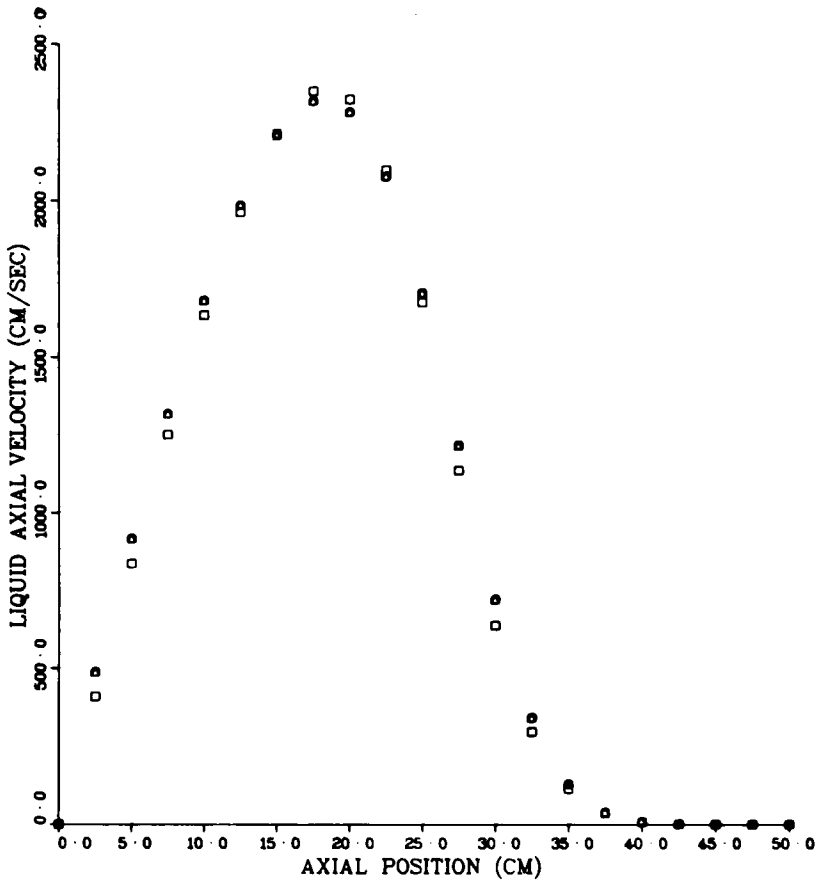

SQUARE IS KPOOL
CIRCLE IS MODIFIED KACHINA
TRIANGLE IS KPOOL1

Fig. 14. Liquid Axial Velocity at 3.5 msec
ANL Neg. No. 116-77-321

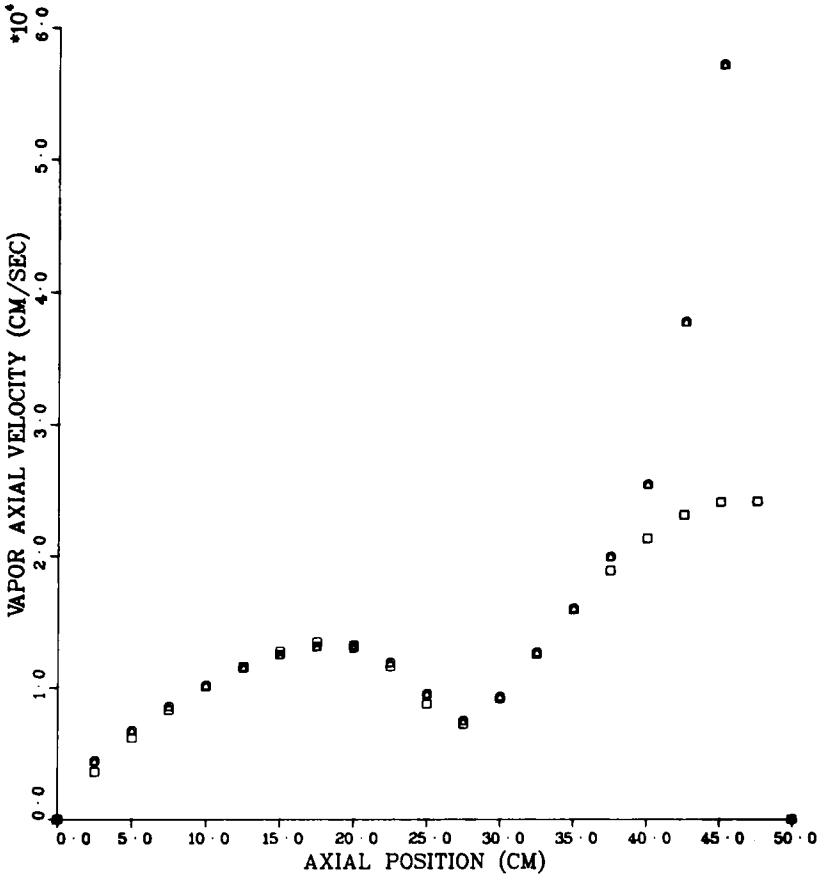

SQUARE IS KPOOL
CIRCLE IS MODIFIED KACHINA
TRIANGLE IS KPOOL1

Fig. 15. Vapor Axial Velocity at 3.5 msec
ANL Neg. No. 116-77-322

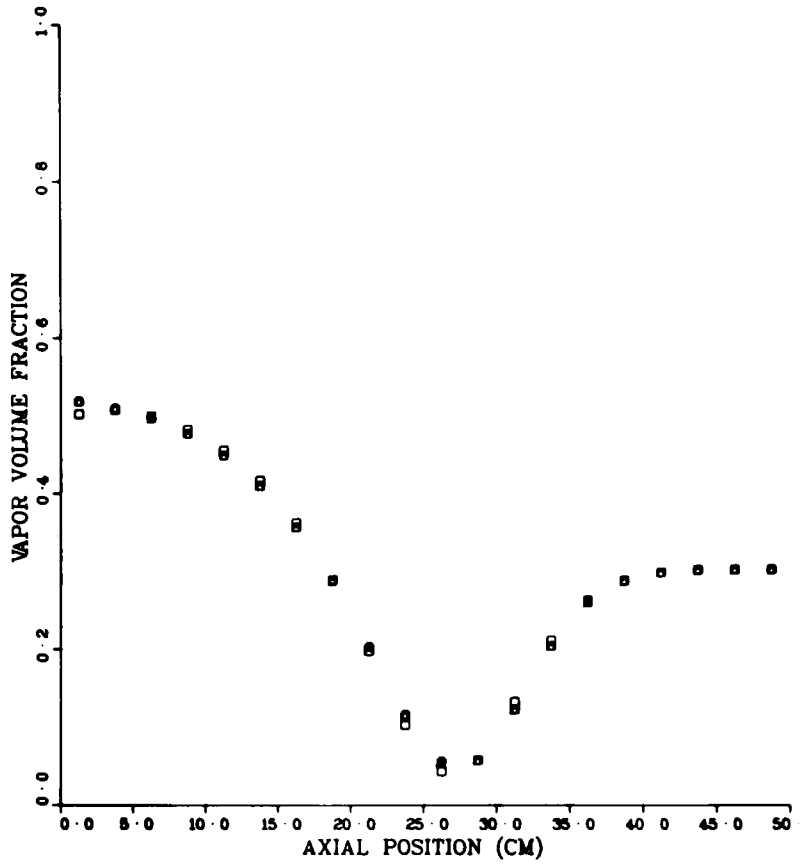

Fig. 16. Vapor Volume Fraction at 3.5 msec
ANL Neg. No. 116-77-323

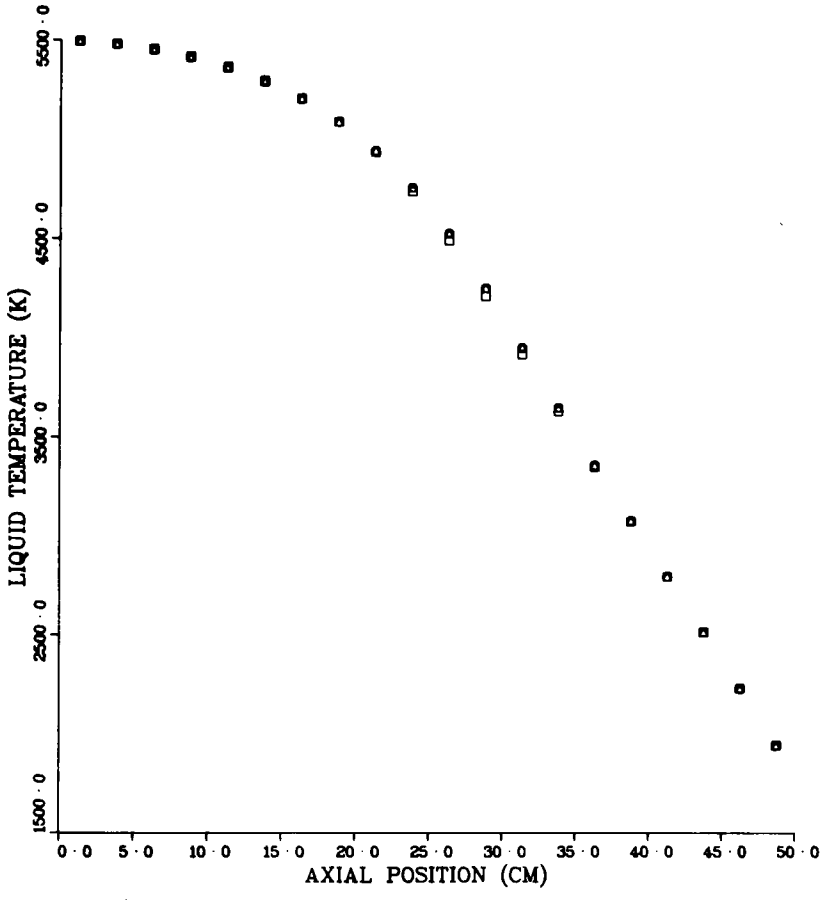

Fig. 17. Liquid Temperature at 3.5 msec
ANL Neg. No. 116-77-324

core. The axial locations of the core midplane, upper axial blanket and lower axial blanket are 0, +50 and -50 cm.

Figures 14-17 show the liquid velocity, vapor velocity, vapor volume fraction, and liquid temperature profiles at 3.5 msec (which is just before the first appearance of single phase regions). This curve shows the maximum observed differences between the codes. As seen from the plots, KPOOL and the modified KACHINA agree very well with the exception of the vapor velocity near the blanket. The upturn in vapor velocity obtained with the modified KACHINA and KPOOL1 is due to the vapor velocity convective term differenced in the KACHINA pure donor cell formulation[13] unphysically balancing the drag term near the blanket. Using KPOOL with its upwind differencing, the drag term is correctly balanced by the pressure gradient.

C. Coordination of RSR Safety Research

1. P. Abramson, H. Hummel and P. Pizzica made a presentation to NRC ARSR in Silver Spring on January 7, 1977 for mid year review.

2. P. Abramson, P. Pizzica and J. Sienicki visited Purdue University for technical discussions and to view the clad relocation simulation experiments with Dr. T. Theofanus on January 20, 1977.

3. P. Abramson, P. Pizzica and J. Sienicki visited Northwestern University on February 28 to discuss simulated boiling fuel/steel pools and view experiments with Dr. G. Bankhoff.

4. P. Abramson & P. Pizzica visited LASL on March 24, 1977 for discussions of heat tranfer effects with J. Jackson and of SIMMER extended motion CDA studies and SIMMER experimental support with J. Boudreau. A recent shift in the LASL proposed SIMMER experimental plan away from basic physics parameter measurements toward macroscopic phenomenologic experimentation has our support.

5. P. Abramson & P. Pizzica visited Sandia on March 25, 1977. P. Pizzic P. Pizzica met with T. Schmidt and was given a tour of the ACPR facilities and consulted with M. Young on EPIC implementation. P. Abramson, held brief technical discussions regarding future experimental plans with M. Young and R. Ostensen and was given a review of the meeting in Paris on FCI's by D. Williams.

6. P. Abramson visited AI on March 31, 1977 for technical discussions on PLBR safety analysis with R. Lancet and J. Mills and for discussions of the Behrens effect analysis with E. Vaughn.

7. P. Abramson visited EPRI on April 1, 1977 for discussions of PLBR HCDA analysis and Behrens effect analysis with E. Fuller.

8. P. Abramson visited D. Cagliostro at SRI on April 1, 1977 to view the experimental facilites for and results of tests to date of the simulated CDA bubble expansion/work energy simulation with water.

Recent experimental results at SRI and recent preliminary analysis with SIMMER both support the previous scoping study results obtained with FX2-POOL

indicating that work energy potential is significantly reduced as the core bubble is formed and expands.

D. Evaluation of Progress in Safety Research

A draft chapter entitled "Reactor Physics Aspects of Safety" with H. H. Hummel as editor has been prepared for a book entitled "The Present Status of Fast Reactor Physics" to be published by NEACRP through the OECD. In this chapter the situation with regard to calculation of reactivity coefficients was reviewed, and the utilization of such coefficients in accident calculations was discussed.

II. MONTE CARLO ANALYSIS AND CRITICALS PROGRAM PLANNING FOR SAFETY-RELATED CRITICALS (A2018)

A. Monte Carlo Analysis of Safety-Related Criticals (E. M. Gelbard)

An input error has been found in the Step 5 VIM computation reported in ANL-77-22. This computation was rerun and we now find that λ (VIM) = 1.010 ± 0.002. For the same core configuration λ S_4-P_1 (TWOTRAN) = 1.013, so that the VIM and S_n eigenvalues agree fairly well. Diffusion theory calculations and S_8-P_0 calculations are now under way. It should be noted that the original diffusion calculation (which gave λ = 1) was run with cross sections not completely compatible with those in our more recent computations.

DOT and TWOTRAN calculations were rerun for Step 1 with reflecting boundary conditions imposed at all outer boundaries of the core. These calculations give

λ_∞ (DOT) = 1.5366

λ_∞ (TWOTRAN) = 1.5371

Apparently, then, if there is any cross section descrepency in the Step 1 DOT and TWOTRAN calculations this discrepancy has no substantial effect on the core k_∞'s. Input data for these S_n calculations are now being processed for transmission to Los Alomos. This processing is not trivial since data, retrieved from storage in an IBM system, must be prepared for use on a CDC machine.

B. Planning of Demo Safety Related Experiments (S. K. Bhattacharyya and L. LeSage)

One of the recommendations of the Fast Reactor Critical Experiment Review Group[14] was to isolate the RSR critical assemblies from the ZPR-9 matrix support structures. As part of the continuing preanalysis program for the critical experiments, the reactivity effects of adding such a reflector were studied. Both depleted uranium and stainless steel reflectors were studied and axial and radial reflector thicknesses of 10 cm and 15 cm were used in each case. The former thickness corresponds to approximately two (2) ZPR drawer widths while the latter is nearly equivalent to three (3) drawer widths. The results of the eigenvalue calculations are summarized in Table II. A 10 cm thick reflector is seen to be effectively infinite for both the depleted uranium and stainless steel. Since the primary purpose of the program of measurements was to validate calculational methods, the depleted uranium reflector was selected to avoid any questions arising from the calculational uncertainties caused by iron and nickel scattering resonances. A reflector thickness of 10 cm was picked.

TABLE II. Results of Eigenvalue Calculations with Reflector

	Reflector Thickness					
	0 cm		10 cm		15 cm	
Reflector Material	Critical Core Radius (cm)	Δk/k on Adding Reflector	Critical Core Radius (cm)	Δk/k on Adding Reflector	Critical Core Radius (cm)	Δk/k on Adding Reflector
Stainless Steel	46.20	0	45.88	0.0027	45.86	0.0030
Depleted Uranium	46.20	0	45.87	0.0027	45.85	0.0029

The real and adjoint fluxes were computed for the reflected reference and fuel slump-in configurations. The central reactivity worths and axial worth traverses of ^{235}U, ^{238}U, ^{239}Pu, ^{240}Pu, sodium and iron were calculated in these two configurations. Such calculations were performed for the unreflec-e ted assemblies (see ANL-76-72). The central reactivity worths of the isotopes are listed in Table III for the two reflected configurations. In addition, the ratios of the reflected worths to the corresponding unreflected values have been presented along with the ratio of the worths in the fuel slump-in and reference configurations. As in the unreflected case, the higher density of fuel and the much smaller perturbation denominator caused the worth of all isotopes to increase in the fuel slump-in configuration relative to the reference configuration. The variation in the ratio of worths indicates the large spectral shifts that occur between the two configurations. The much harder spectrum in the fuel slump-in case causes an increase in the fission source component of the worths of ^{238}U and ^{240}Pu and this is clearly observed in the ratio.

The reactivity worths of these materials as a function of axial position are listed in Tables IV-IX and shown graphically in Figs. 18-23. The axial worth profiles are generally similar to the corresponding unreflected cases, although the effect of the axial reflector is clearly more pronounced for the slump-in configuration because of the voided region between the core and the reflector.

TABLE III. Central Material Worths for the Reference and Fuel Slump-In Configurations with Depleted Uranium Reflector

Parameter	Reference Configurations (Step 1)	Ratio $\frac{\text{Reflected}^a}{\text{Unreflected}}$	Fuel Slump-In Configuration (Step 4)	Ratio $\frac{\text{Reflected}}{\text{Unreflected}}$	$\frac{\text{Step 4}}{\text{Step 1}}$
Prompt Neutron Lifetime (Sec)	3.2375×10^{-7}	0.99	2.3772×10^{-7}	1.12	0.7343
β_{eff}	3.1505×10^{-3}	1.01	3.3064×10^{-3}	1.00	1.0495
Reactivity Conversion Factor (Ih/%ρ)	9.8224×10^{-2}	1.00	9.5981×10^{-2}	1.00	0.9772
Material Worths Ih/kg					
^{235}U	364.95	1.07	693.94	0.92	1.9015
^{238}U	-23.99	1.07	-30.44	0.88	1.2689
^{239}Pu	500.92	1.07	1035.61	0.92	2.0674
^{240}Pu	85.34	1.07	262.98	0.92	3.0816
Na	-22.34	1.07	-51.31	0.91	2.2968
Fe	-13.04	1.07	-31.08	0.91	2.3834

[a]Unreflected data from ANL-76-72, page 25.

TABLE IV. ^{235}U Axial Reactivity Worth Traverse, Ih/kg

HEIGHT ABOVE MIDPLANE	STEP 1. (REFERENCE)	STEP 4. (SLUMPED)
0.8880	364.9458	693.9407
2.6640	363.4988	683.9314
4.4400	360.6177	664.1584
6.2160	356.3274	635.1262
7.9920	350.6782	597.5361
9.7680	343.6953	552.3953
11.5440	335.4543	500.9224
13.3200	326.0181	444.5798
15.0960	315.4746	385.1138
16.8720	303.9119	324.4678
18.6480	291.4434	264.7925
20.4240	278.1697	208.4012
22.2000	264.5686	157.6535
24.3707	247.7471	130.3060
26.9361	226.6098	121.8276
29.5015	204.6798	114.6342
32.0669	182.7624	108.3236
34.6323	161.2979	102.6205
37.1977	140.7268	97.3440
39.7631	121.4893	92.3848
42.3285	104.0787	87.6876
44.8939	89.0448	83.2363
47.5859	76.4756	79.0530
50.4045	63.9618	75.1870
53.2231	52.3728	71.7071
56.0417	42.0205	64.7017
58.8603	33.5454	54.2718
61.6789	26.4481	44.8023
64.0502	21.3084	36.4862
65.9742	17.8258	29.3690
67.8982	14.8968	23.3978
69.8222	12.3648	18.4632
71.7462	10.1912	14.4373
73.6702	8.3357	11.1850
75.5942	6.7603	8.5814
77.5182	5.4294	6.5138
79.4422	4.3104	4.8842
81.3662	3.3738	3.6084
83.2902	2.5933	2.6164
85.2142	1.9587	1.8493
87.8431	0.7422	0.8569
91.1764	0.1752	0.2506
94.5097	0.0241	0.0391

TABLE V. ^{238}U Axial Reactivity Worth Traverse, Ih/kg

HEIGHT ABOVE MIDPLANE	STEP 1. (REFERENCE)	STEP 4. (SLUMPED)
0.8880	-23.9926	-31.4397
2.6640	-23.8721	-30.6093
4.4400	-23.6336	-28.9593
6.2160	-23.2783	-26.5104
7.9920	-22.8100	-23.2954
9.7680	-22.2311	-19.3580
11.5440	-21.5478	-14.7540
13.3200	-20.7664	-9.5519
15.0960	-19.8930	-3.8363
16.8720	-18.9365	2.2890
18.6480	-17.9041	8.6986
20.4240	-16.8047	15.2445
22.2000	-15.3015	21.7644
24.3707	-12.9697	22.8595
26.9361	-10.4995	19.5438
29.5015	-8.3585	17.0815
32.0669	-6.2166	15.1365
34.6323	-4.1164	13.4744
37.1977	-2.0997	11.9347
39.7631	-0.2083	10.4153
42.3285	1.5176	8.8570
44.8939	2.9730	7.2382
47.5859	3.1084	5.5689
50.4045	2.2826	3.8871
53.2231	1.3227	2.2526
56.0417	0.3982	1.3714
58.8603	0.0976	1.2522
61.6789	-0.0575	1.0660
64.0502	-0.2784	0.8602
65.9742	-0.3061	0.6676
67.8982	-0.2376	0.5040
69.8222	-0.1835	0.3731
71.7462	-0.1410	0.2724
73.6702	-0.1078	0.1967
75.5942	-0.0819	0.1407
77.5182	-0.0619	0.0997
79.4422	-0.0465	0.0698
81.3662	-0.0346	0.0482
83.2902	-0.0255	0.0325
85.2142	-0.0062	0.0213
87.8431	0.0164	0.0202
91.1764	0.0129	0.0173
94.5097	0.0098	0.0163

TABLE VI. ^{239}Pu Axial Reactivity Worth Traverse, Ih/kg

HEIGHT ABOVE MIDPLANE	STEP 1. (REFERENCE)	STEP 4. (SLUMPED)
0.8880	500.9226	1035.6077
2.6640	498.9067	1020.3254
4.4400	494.9229	990.1362
6.2160	488.9724	945.7524
7.9920	481.1174	888.2507
9.7680	471.4185	819.0823
11.5440	459.9631	740.0720
13.3200	446.8499	653.4207
15.0960	432.1777	561.6914
16.8720	416.0833	467.8345
18.6480	398.7021	375.1621
20.4240	380.1829	287.2898
22.2000	361.0203	208.0017
24.3707	337.1196	166.2660
26.9361	307.1821	155.1308
29.5015	276.1807	145.5311
32.0669	245.0556	137.0195
34.6323	214.3881	129.3058
37.1977	184.7598	122.1726
39.7631	156.7520	115.5181
42.3285	130.9709	109.2649
44.8939	108.0303	103.4012
47.5859	88.1218	97.9436
50.4045	70.6750	92.9407
53.2231	55.8535	88.4600
56.0417	43.4739	78.3017
58.8603	33.7911	63.5878
61.6789	26.0346	50.9691
64.0502	20.6334	40.4094
65.9742	17.0521	31.7443
67.8982	14.0967	24.7380
69.8222	11.5896	19.1390
71.7462	9.4730	14.7030
73.6702	7.6934	11.2152
75.5942	6.2032	8.4903
77.5182	4.9600	6.3735
79.4422	3.9268	4.7383
81.3662	3.0715	3.4819
83.2902	2.3658	2.5214
85.2142	1.7984	1.7906
87.8431	0.7173	0.8548
91.1764	0.1769	0.2557
94.5097	0.0244	0.0396

TABLE VII. ^{240}U Axial Reactivity Worth Traverse, Ih/kg

HEIGHT ABOVE MIDPLANE	STEP 1. (REFERENCE)	STEP 4. (SLUMPED)
0.8880	85.3394	262.9756
2.6640	85.0117	259.2671
4.4400	84.3588	251.9592
6.2160	83.3856	241.1955
7.9920	82.0995	227.2653
9.7680	80.5103	210.5057
11.5440	78.6304	191.3623
13.3200	76.4721	170.3767
15.0960	74.0526	148.1751
16.8720	71.3905	125.5040
18.6480	68.5029	103.2109
20.4240	65.4132	82.2554
22.2000	62.4825	63.7380
24.3707	59.1552	52.1135
26.9361	54.5884	46.6618
29.5015	49.4772	42.2685
32.0669	44.2539	38.5710
34.6323	38.9924	35.3154
37.1977	33.7630	32.3271
39.7631	28.6345	29.4966
42.3285	23.6835	26.7599
44.8939	18.9530	24.0906
47.5859	13.8578	21.4973
50.4045	9.6769	19.0134
53.2231	6.4532	16.6981
56.0417	3.9939	13.4883
58.8603	2.6288	10.1239
61.6789	1.7326	7.5136
64.0502	1.0709	5.5229
65.9742	0.7636	4.0296
67.8982	0.6098	2.9247
69.8222	0.4880	2.1154
71.7462	0.3911	1.5264
73.6702	0.3135	1.0996
75.5942	0.2512	0.7910
77.5182	0.2011	0.5682
79.4422	0.1607	0.4073
81.3662	0.1281	0.2913
83.2902	0.1017	0.2077
85.2142	0.0929	0.1474
87.8431	0.0628	0.0849
91.1764	0.0245	0.0363
94.5097	0.0105	0.0176

TABLE VIII. Sodium Axial Reactivity Worth Traverse, Ih/kg

HEIGHT ABOVE MIDPLANE	STEP 1. (REFERENCE)	STEP 4. (SLUMPED)
0.8880	-22.3366	-51.3094
2.6640	-22.1398	-48.7032
4.4400	-21.7488	-43.5035
6.2160	-21.1648	-35.7404
7.9920	-20.3956	-25.4567
9.7680	-19.4463	-12.7126
11.5440	-18.3246	2.4115
13.3200	-17.0396	19.8119
15.0960	-15.6041	39.3473
16.8720	-14.0284	60.8414
18.6480	-12.3260	84.0804
20.4240	-10.5130	108.8519
22.2000	-7.0640	135.0214
24.3707	-0.7999	131.5013
26.9361	5.1462	114.7280
29.5015	9.5531	102.0166
32.0669	13.9744	91.7957
34.6323	18.3156	82.9565
37.1977	22.4717	74.7471
39.7631	26.3164	66.6835
42.3285	29.6840	58.4917
44.8939	32.0457	50.0673
47.5859	28.3282	41.4543
50.4045	20.8072	32.8288
53.2231	13.4239	24.4673
56.0417	6.9741	17.7112
58.8603	3.9600	14.3105
61.6789	2.1043	11.1447
64.0502	0.4558	8.4082
65.9742	-0.0844	6.1826
67.8982	-0.1078	4.4551
69.8222	-0.1151	3.1606
71.7462	-0.1125	2.2148
73.6702	-0.1041	1.5368
75.5942	-0.0929	1.0572
77.5182	-0.0806	0.7213
79.4422	-0.0685	0.4875
81.3662	-0.0573	0.3255
83.2902	-0.0474	0.2136
85.2142	0.0133	0.1363
87.8431	0.0774	0.1035
91.1764	0.0572	0.0804
94.5097	0.0438	0.0749

TABLE IX. Iron Axial Reactivity Worth Traverse, Ih/kg

HEIGHT ABOVE MIDPLANE	STEP 1. (REFERENCE)	STEP 4. (SLUMPED)
0.8880	-13.0437	-31.0784
2.6640	-12.9526	-29.9874
4.4400	-12.7720	-27.8143
6.2160	-12.5025	-24.5762
7.9920	-12.1467	-20.2999
9.7680	-11.7077	-15.0211
11.5440	-11.1888	-8.7860
13.3200	-10.5946	-1.6547
15.0960	-9.9301	6.2921
16.8720	-9.1999	14.9451
18.6480	-8.4114	24.1554
20.4240	-7.5706	33.7198
22.2000	-6.1260	43.3608
24.3707	-3.6078	44.9392
26.9361	-1.1413	39.1476
29.5015	0.7824	34.7854
32.0669	2.7243	31.3004
34.6323	4.6506	28.3034
37.1977	6.5253	25.5305
39.7631	8.3055	22.8125
42.3285	9.9343	20.0520
44.8939	11.1538	17.2113
47.5859	10.1011	14.3054
50.4045	7.5192	11.3933
53.2231	4.9967	8.5702
56.0417	2.7611	6.5601
58.8603	1.6829	5.4288
61.6789	0.9820	4.3254
64.0502	0.3526	3.3397
65.9742	0.1317	2.5156
67.8982	0.0998	1.8590
69.8222	0.0753	1.3537
71.7462	0.0566	0.9744
73.6702	0.0424	0.6947
75.5942	0.0316	0.4911
77.5182	0.0235	0.3443
79.4422	0.0174	0.2392
81.3662	0.0128	0.1645
83.2902	0.0094	0.1117
85.2142	0.0263	0.0745
87.8431	0.0391	0.0491
91.1764	0.0228	0.0314
94.5097	0.0153	0.0256

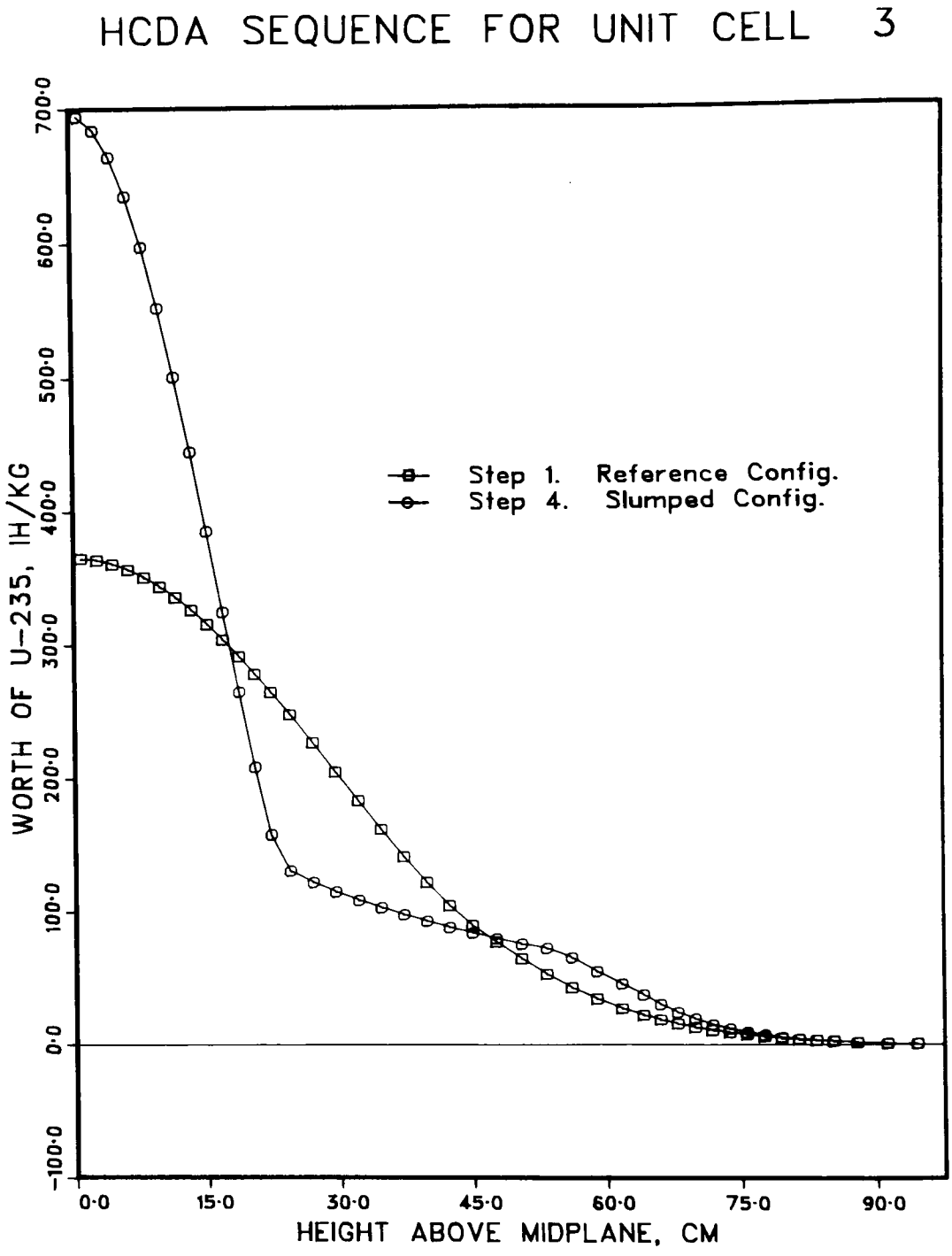

Fig. 18. ^{235}U Axial Reactivity Worth Traverse
ANL Neg. No. 116-77-405

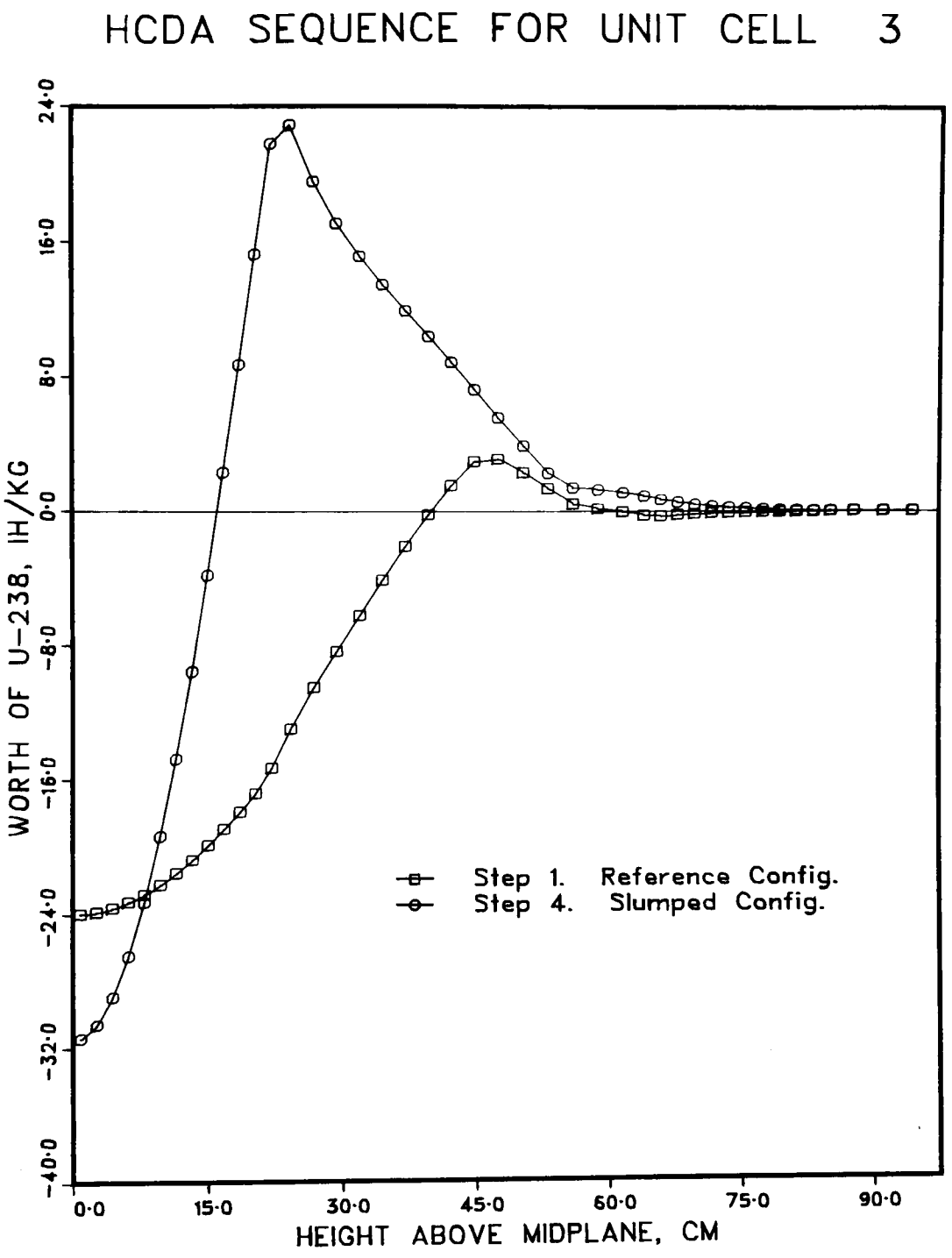

Fig. 19. ^{238}U Axial Reactivity Worth Traverse
ANL Neg. No. 116-77-403

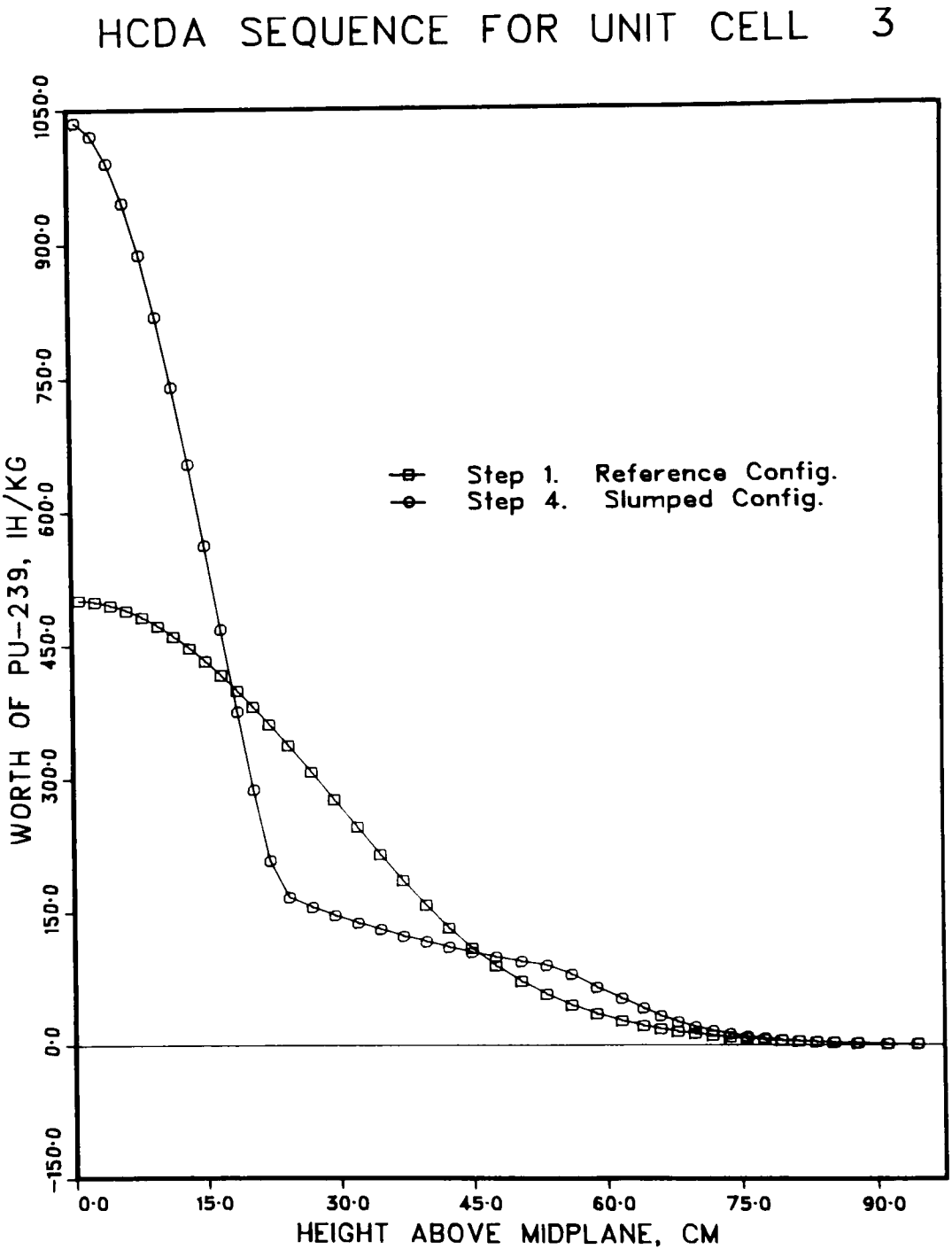

Fig. 20. ^{239}U Axial Reactivity Worth Traverse
ANL Neg. No. 116-77-408

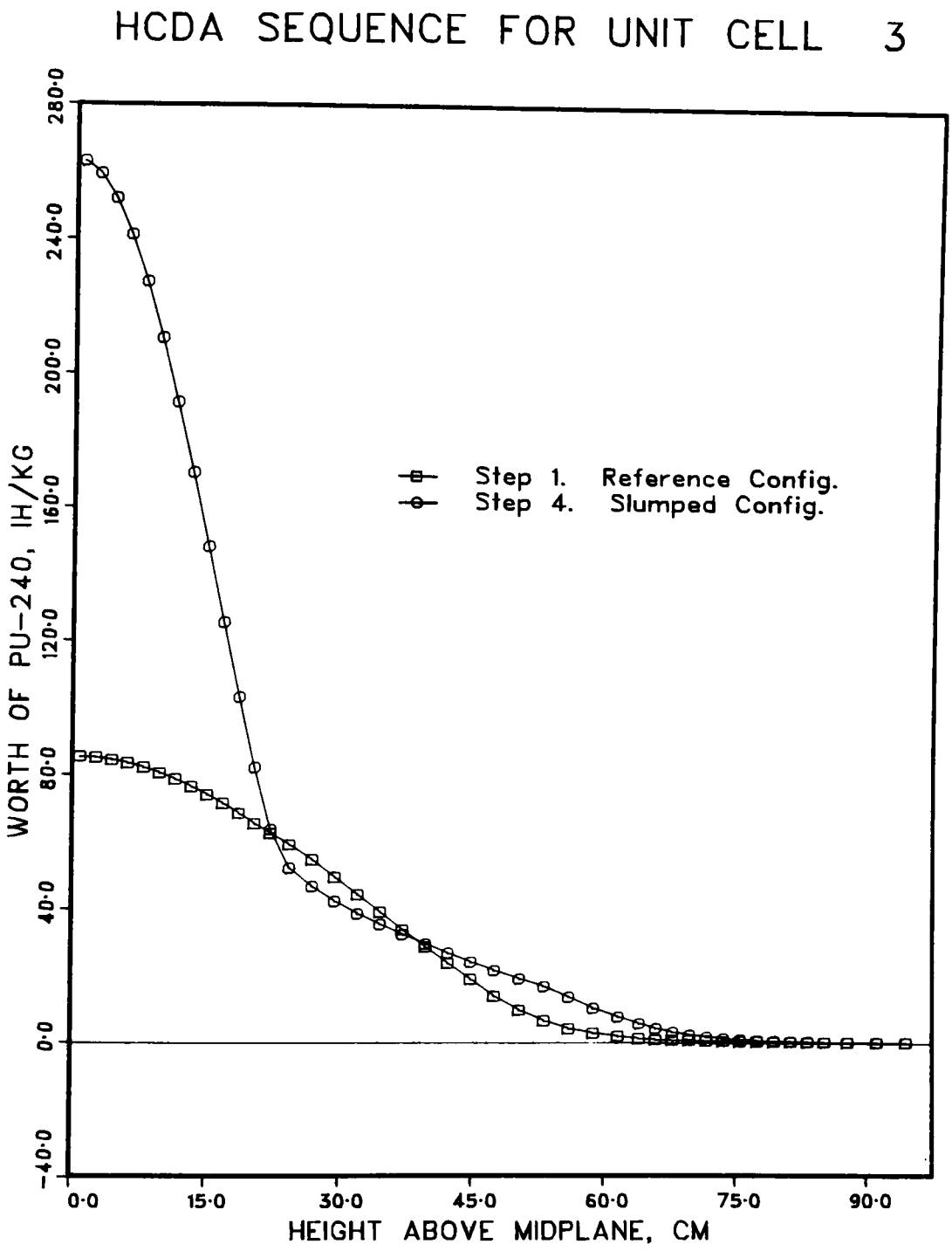

Fig. 21. ^{240}U Axial Reactivity Worth Traverse
ANL Neg. No. 116-77-409

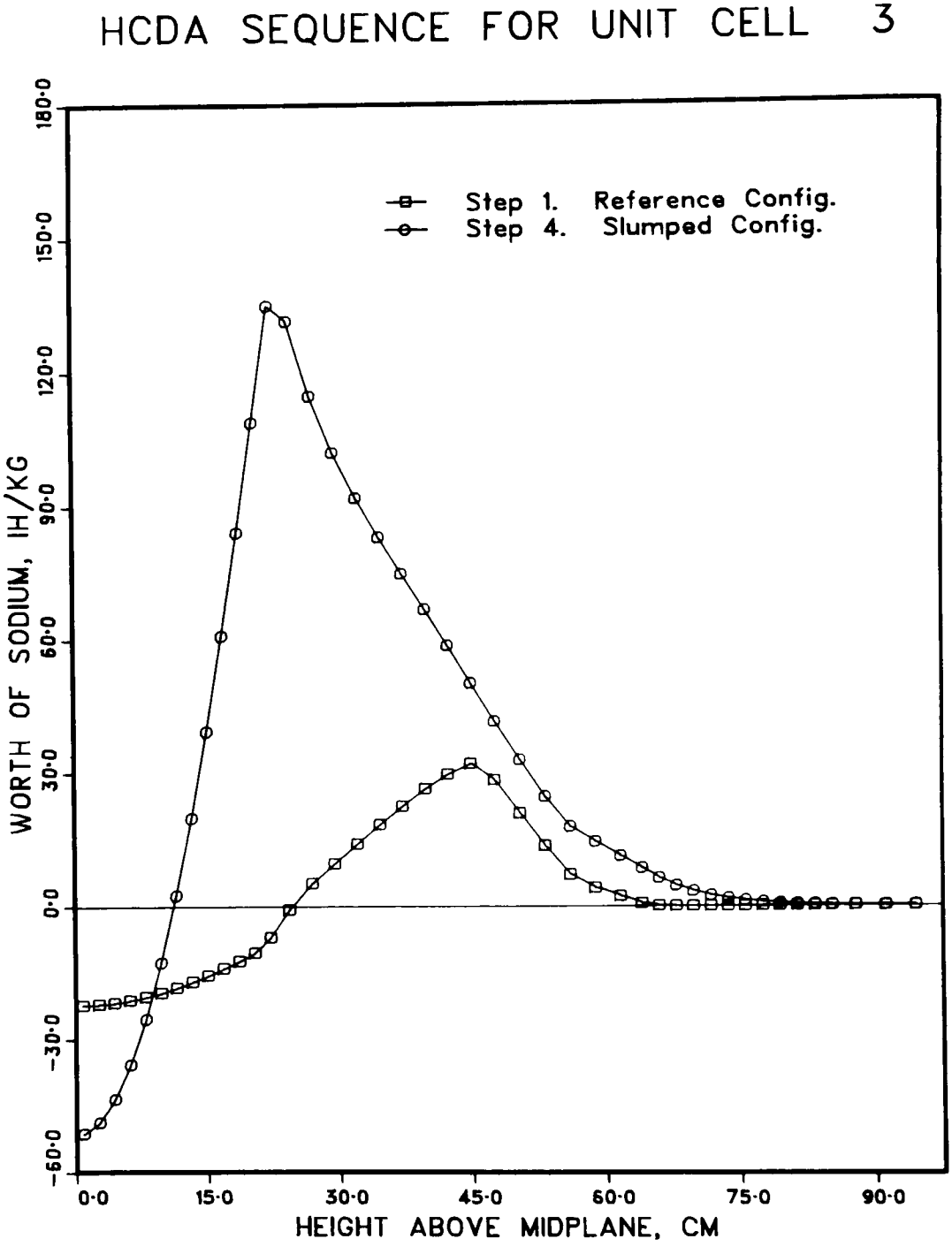

Fig. 22. Sodium Axial Reactivity Worth Traverse
ANL Neg. No. 116-77-411

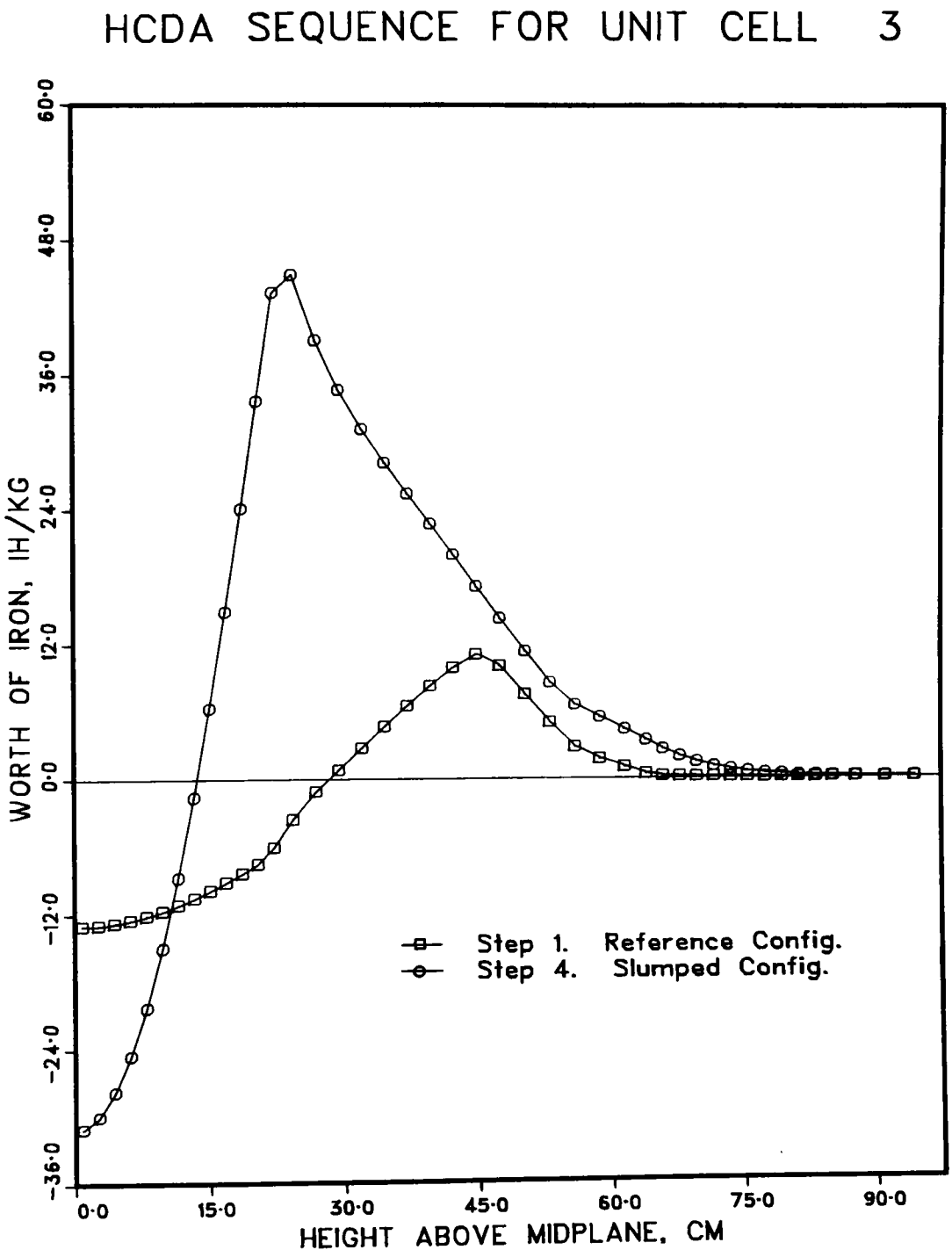

Fig. 23. Iron Axial Reactivity Worth Traverse
ANL Neg. No. 116-77-410

III. THREE-DIMENSIONAL CODE DEVELOPMENT FOR CORE THERMAL HYDRAULIC ANALYSIS OF LMFBR ACCIDENTS UNDER NATURAL CONVECTION CONDITIONS (A2045)

A. Introduction (W. T. Sha and H. M. Domanus)

Any computer program development of thermal hydraulic analyses must begin with a relationship between the grid system and the geometric configuration. The relationship chosen sets the limits of possible applications and effects virtually all programming details of the code. In the COMMIX code[15] development, a staggered mesh system is being employed in finite differencing the governing differential equations. A methodology has been developed to extend applications of the staggered mesh system to complicated three-dimensional geometrical configurations.

The methodology presented here employs x-y-z cartesian coordinates and modifies the finite differencing equations[16] to resolve irregular three-dimensional geometrical configurations in a staggered mesh system. More important, it lends itself to a consistant approach to handle various types of boundary conditions.

B. Geometric Configuration Specification

The geometrical configuration is specified by considering a collection of bounded finite surfaces. The collection of surfaces forms a closed finite volume referred to as the region of interest.

Each component surface is defined by the following specifications:

1. A three-dimensional rectangular box defining a closed subregion containing the surface.

2. A function $f(x,y,z) = 0$ defining the coordinates of a surface point.

3. A function $g(x,y,z) \geq 0$ or both functions $g(x,y,z) \geq 0$ and $h(x,y,z) \geq 0$ to further define the extent of the surface $f(x,y,z)$.

The location of the origin of a cartesian coordinate system is chosen such that all coordinates in the region of interest are positive. Once the origin has been established, coordinates and functions defining surfaces can be determined. The total number of surfaces, NSURF, used to characterize the region of interest is then determined. Consider the pipe section shown in Fig. 24. The pipe is of radius 2 meters and is 5 meters long. It can be characterized by three surfaces as indicated. A box containing surface 1 is specified by

XMIN (1) = 0.0	XMAX (1) = 6.0
YMIN (1) = 0.0	YMAX (1) = 6.0
ZMIN (1) = 4.0	ZMAX (1) = 6.0

Because surface 1 may be uniquely defined using the f & g function definitions, the coarseness of the three-dimensional rectangular box is irrelevant.

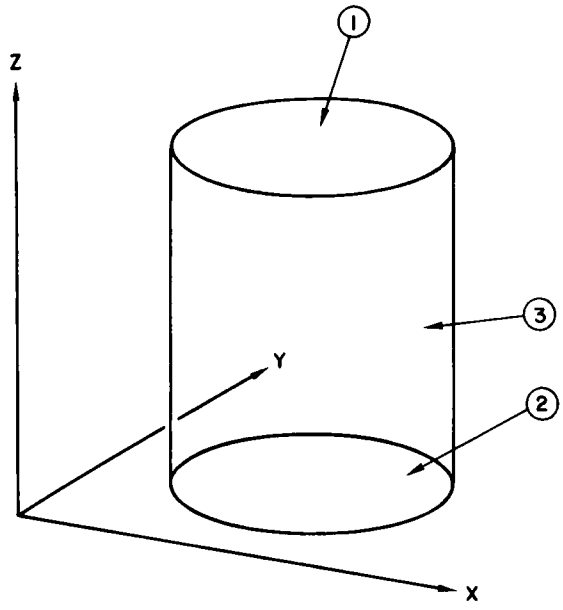

Fig. 24. Geometric Specification of a Pipe Section
ANL Neg. No. 116-77-402

The f(x,y,z) function defines the surface. In addition to relating coordinates of a surface point, f(x,y,z) also carries surface normal information. If point B = (XB,YB,ZB) is located on the surface then f(XB,YB,ZB) = 0.0, and a unit normal vector $\hat{n}$ (XB,YB,ZB) = XN,YN,ZN is pointing from point B into the region of interest. The coordinates of the unit normal vector are given by

$$XN = \frac{1}{||N||} \frac{\partial f}{\partial x} (XB,YB,ZB)$$

$$YN = \frac{1}{||N||} \frac{\partial f}{\partial y} (XB,YB,ZB)$$

$$ZN = \frac{1}{||N||} \frac{\partial f}{\partial z} (XB,YB,ZB)$$

where $||N||$ is:

$$||N|| = \sqrt{\left(\frac{\partial f}{\partial x}\right)^2 + \left(\frac{\partial f}{\partial y}\right)^2 + \left(\frac{\partial f}{\partial z}\right)^2}$$

The functional form of f(x,y,x) is defined as:

$$\begin{aligned} f(x,y,z) &= (FX2)\, x^2 + (FX)\, x + (FY2)\, y^2 + (FY)\, y \\ &+ (FZ2)\, z^2 + (FZ)\, z + (FXY)\, xy + (FXZ)\, xz \\ &+ (FYZ)\, yz + FC = 0. \end{aligned}$$

This functional form appears adequate for defining surfaces of current interest (i.e., cylinders, hexagonal fuel assembly can wall, planes, piping tees, elbows,

etc.). However, more complicated functions such as cubic polynominals in x, y and z can readily be incorporated, if it is found to be necessary.

The appropriate f function to define surface 1 of Fig. 24 is

$$f(x,y,z) = -x + 5 = 0 \text{ or equivalently}$$
$$FZ(1) = -1 \text{ and } FC(1) = 5, \text{ other f coefficients} = 0.$$

The unit surface normal is $\hat{n} = (0,0,-1)$ indicating the region of interest is located below the plane $z = 5$.

The g(x,y,z) function definition limits the extent of the surface. The functional form used is:

$$g(x,y,z) = (GX2)\,x^2 + (GX)\,x + (GY2)\,Y^2 + (GY)\,y + (GZ2)\,z^2 + (GZ)\,z + (GXY)\,xy + (GXZ)\,xy + (GYZ)\,yz + GC \geq 0.0.$$

The appropriate g function to complete the definition of surface 1 in Fig. 24 is:

$$g(x,y,z) = -x^2 + 6x - y^2 + 6y - 14 \geq 0 \text{ or}$$
$$GX2(1) = -1,\ GX(1) = 6,$$
$$GY2(1) = -1,\ GY(1) = 6,\ GC(1) = -14,$$

other g coefficients = 0. The g function definition gives surface 1 its circular shape, since every point B = (XB,YB,ZB) on the surface f(XB,YB,ZB) = 0 must satisfy

$$g(XB,YB,ZB) \geq 0.0$$

The function h(x,y,z) also imposes a restriction on the extent of the surface. The functional form is:

$$h(x,y,z) = (HX2)\,x^2 + (HX)\,x + (HY2)\,y^2 + (HY)\,y + (HZ2)\,z^2 + (HZ)\,z + (HXY)\,xy + (HXZ)\,xz + (HYZ)\,yz + HC \geq 0.0.$$

Use of the g and h functions is optional, but when irregularly shaped surfaces are required these functions are needed. The h(x,y,z) function limitation is not needed in the example specification of surface 1 in Fig. 24. Therefore, all h coefficients are set equal to zero. Similiarly, surfaces 2 and 3 of Fig. 24 are specified by:

$$XMIN(2) = 0, \quad XMAX(2) = 6$$
$$YMIN(2) = 0, \quad YMAX(2) = 6$$
$$ZMIN(2) = -1, \quad ZMAX(2) = 1$$
$$FX(2) = 1, \text{ other f coefficients} = 0$$
$$FX2(2) = -1,\ GX(2) = 6,$$
$$GY2(2) = -1,\ GY(2) = 6,\ GC(2) = -14, \text{ other g coefficients} = 0$$

and

XMIN(3) = 0, XMAX(3) = 6
YMIN(3) = 0, YMAX(3) = 6
ZMIN(3) = 0, ZMAX(3) = 5
FX2 (3) = -1, FX(3) = 6,
FY2 (3) = -1, FY(3) = 6, FC (3) = -14, other f coefficients = 0
all g and h coefficients = 0.

C. Grid Definition

Once the geometrical configuration has been defined in detail as outlined in Sect. B, a grid is imposed to approximately resolve the region of interest. The grid is a staggered mesh system.

After determining the dimensions of a rectangular box completely enclosing the region of interest, a partitioning of each of the three sides of the box in the x, y and z directions is chosen. There are IMAX, JMAX and KMAX number of partitions in the x, y and z directions, respectively. The length of the Ith partition in the x direction is specified by DX(I). Similarly, DY(J) and DZ(K) are the lengths of the Jth and Kth partitions in the y and z directions, respectively. The overall dimensions of the box are:

$$\text{length in x dimension} = \sum_{I=1}^{IMAX} DX(I)$$

$$\text{length in y dimension} = \sum_{J=1}^{JMAX} DY(J) \text{ and}$$

$$\text{length in z dimension} = \sum_{K=1}^{KMAX} DZ(K).$$

From this partitioning, four different grids are considered for a staggered mesh system. Each grid may be viewed as the intersection points of three orthogonal line systems, parallel to the x, y and z axes, respectively. The four grids are referred to as the field points or grid, U points, V points or W points.

Discrete locations are defined in terms of

X(1) = 1/2 DX(1)
X(1) = X(I-1) + 1/2 DX(I-1) + DX(I) , I = 2, IMAX
Y(1) = 1/2 DY(1)
Y(J) = Y(J-1) + 1/2 DY(J-1) + DY(J) , J = 2, JMAX

and

Z(1) = 1/2 DZ(1)
Z(K) = Z(K-1) + 1/2 DZ(K-1) + DZ(K) , K = 2, KMAX.

Field points have coordinates

$$(X(I), Y(J), Z(K)),$$

U points have coordinates

$$(X(I) + 1/2\ DX(I), Y(J), Z(K)),$$

V points have coordinates

$$(X(I), Y(J) + 1/2\ DY(J), Z(K)) \text{ and}$$

W points have coordinates

$$(X(I), Y(j), Z(K) + 1/2\ DZ(K)),\ I = 1, IMAX,\ J = 1, JMAX,\ K = 1, KMAX.$$

For example, consider field points y and z fixed. These field points all lie on a line referred to as a CX line, parallel to the x axis. (The set of CX lines is defined for a given J and K where J = 1, JMAX and K = 1, KMAX.) Similarly, CY and CZ lines are defined, respectively, parallel to the y and z axes. Intersections of CX, CY and CZ lines define field points.

A similiar system is considered for U points with UX, UY and UZ lines. Intersections of these lines define U points. Similarly, VX, VY and VZ lines for V points and WX, WY and WZ lines for W points are considered. The field grid locates discrete points of the field variables (i.e., pressure, temperature, density). The U, V and W grids, respectively, locate discrete points of velocity components. Because of the relationship between field and velocity points in the staggered mesh system, some of these lines are redundant. In particular,

CX lines = UX lines
CY lines = VY lines and
CZ lines = WZ lines.

D. Identification of Internal and Surface Intersection Grid Points

The rectangular box completely enclosing the region of interest has been partitioned and resolved by IMAX * JMAX * KMAX number grid points as described in Sect. C. These grid points (i.e., IMAX * JMAX & KMAX) may be more than the number needed to resolve the internal region of interest. Only points inside the region of interest need be considered. Because of the potentially large computer storage requirements in three dimensional finite difference calculations, it is desirable to eliminate all grid points outside the region of interest. This is accomplished by identifying and labeling grid points inside the region of interest with a counter M. Each point M has a IJK(M) position identifier associated with it as

$$IJK(M) = iijjkk$$

so that I,J,K can be recovered by the relations

$$I = IJK(M)/10000$$
$$J = (IJK(M) - 10000 * I)/100$$
$$K = IJK(M) - 10000 * I - 100 * J$$

using FORTRAN fixed point arithmetic. The spacial position of point M can be obtained from the I, J, K set as

field point: (X(I), Y(J), Z(K))
U point: (X(I) + 1/2 DX(I), Y(J), Z(K))
V point: (X(I), Y(J) + 1/2 DY(J), Z(K))
W point: (X(I), Y(J), Z(K) + 1/2 DZ(K)).

All internal field points are identified and numbered from M = 1, NM. It may happen that a velocity point is inside the region of interest while the related field point is not. Such points are identified and labeled M = NM + 1, NML. If the region of interest deviates from the enclosing rectangular box, (IMAX * JMAX * KMAX - NM) number of storage locations will have been eliminated from further considerations.

In addition to identifying internal points, points of surface intersection with CX, CY, CZ, UY, UZ, VX, VZ, WX and WY lines are idetified and labeled with counter L, where L = 1, NL. Each point L is located at coordinates (XB(L), YB(L), ZB(L)) and has local surface nominal $\hat{n}$ = (XN(L), YN(L), ZN(L)). Surface intersection points are classified as to the type of line generating it as well as being associated with the particular intersecting surface, N. This information is summarized and stored by the LCX(N), LCY(N), LCZ(N), LUY(N), LUZ(N), LVX,(N), LVZ(N), LWX(N) and LWY(N), N = 1, NSURF arrays as indicated by Table X.

E. Positional Relationships between Internal and Surface Points

In addition to identifying and locating internal and surface points, positional relationships between one internal point and its neighbors (either internal or surface) are determined. Some arbitrary conventions are introduced to communicate this information within the computer code. Positional relationships among field points are summarized by the 6 arrays MIM(M), MIP(M), MJM(M), MJP(M), MKM(M) and MKP(M). The MIM(M) array refers to the adjacent field point in the minus x direction along a CX line. Similarly, MIP(M) refers to the adjacent field point in the positive x direction along a CX line. The other arrays have similar meanings along minus and plus CY and CZ lines, respectively. Figures 25 and 26 show the relationships between field points F(M) and their corresponding spacial locations. Values of these arrays indicate whether the adjacent field point is inside, outside or a surface point, as well as the particular M or L value of the adjacent field or surface point.

While the MIM, MIP, MJM, etc., arrays also indicate positional relationships between internal U, V and W points, they do not carry information of surface points derived from UY, UZ, VX, VZ, WX or WY line intersections. To accommodate the information, the JU(M), KU(M), IV(M), KV(M), IW(M) and JW(M) arrays are, respectively, introduced. These arrays indicate whether the U, V or W point, M is inside, outside or adjacent to a surface point, and if adjacent to a surface point, the particular L value the surface point is labeled.

Adjacent internal field, U, V or W points from a surface point, L, along the appropriate CX, CY, CZ, UY, UZ, VX, WX or WY line are contained in the MB(L) array. This information is useful in boundary condition calculations in which surface values are related to internal values.

TABLE X. Associated Surface Points with L Counter

Line Type	Surface No.	L Value Beginning	Ending
CX	1	1	LCX(1)
CY	1	LCX(1) + 1	LCY(1)
CZ	1	LCY(1) + 1	LCZ(1)
CX	2	LCZ(1) + 1	LCX(2)
CZ	2	LCX(2) + 1	LCY(2)
.	.	.	.
.	.	.	.
.	.	.	.
CZ	NSURF	LCY(NSURF) + 1	LCZ(NSURF)
UY	1	LCZ(NSURF) + 1	LUY(1)
UZ	1	LUY(1) + 1	LUZ(1)
VX	1	LUZ(1) + 1	LVX(1)
VZ	1	LVX(1) + 1	LVZ(1)
WX	1	LVZ(1) + 1	LWX(1)
WY	1	LWX(1) + 1	LWY(1)
UY	2	LWY(1) + 1	LUY(2)
UZ	2	LUY(2) + 1	LUZ(2)
.	.	.	.
.	.	.	.
.	.	.	.
WX	NSURF	LVZ(NSURF) + 1	LWX(NSURF)
WY	NSURF	LWX(NSURF) + 1	LWY(NSURF) = NL

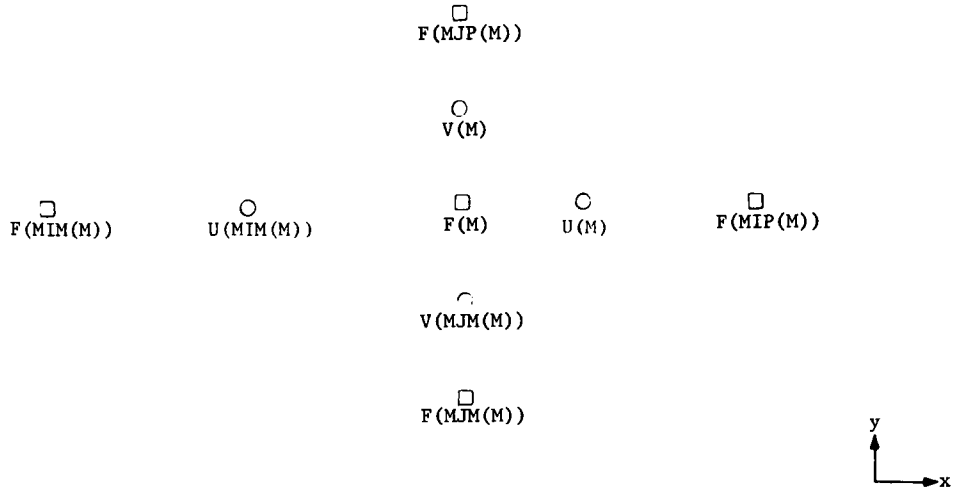

Fig. 25. Positional Relationship Between Internal Points in x-y Plane
ANL Neg. No. 116-77-407

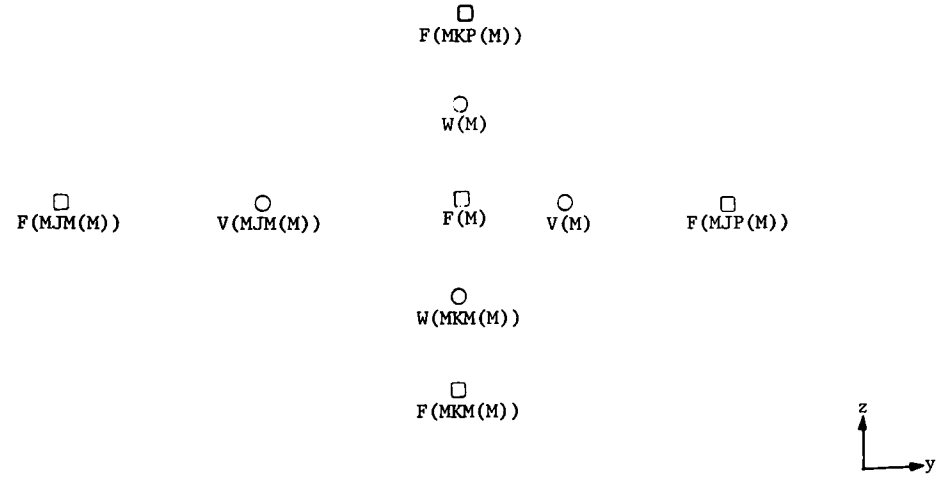

Fig. 26. Positional Relationship Between Internal Points in y-z Plane
ANL Neg. No 116-77-406

F. Conclusion

The methodology presented in this report has the following unique features:

1. Optimizing the computer storage utilization.

2. Providing flexibility of describing the complicated three-dimensional configurations (such as cylinder, hexagonal fuel assembly duct wall, planes, piping tee, elbow etc.) encountered in engineering applications with the xyz cartesian coordinates.

REFERENCES

1. P. A. Pizzica and P. B. Abramson, *"EPIC: A Computer Code for Fuel-Coolant Interaction,"* Proc. of International Meeting on Fast Reactor Safety and Related Physics, Chicago (October 1976).

2. T. P. McLachlan, *"Effects of Neutron Streaming and Geometric Models on Molten Fuel Recriticality Accidents,"* TANSAO 22, p. 372 (1975).

3. R. B. Nicholson, *"Design Basis Accident Studies: Final Report,"* Parts 4 and 5, COO-2286-3, June 22, 1974.

4. E. L. Fuller, EPRI 1976, personal communications.

5. W. T. Sha & T. H. Hughes, *"VENUS: A Two Dimentional Coupled Neutronics - Hydrodynamic's Computer Program for Fast Reactor Power Exursions,"* ANL 7701, Argonne National Laboratory (1972).

6. D. J. Behrens, *"The Effect of Holes in a Reacting Material on the Passage of Neutrons,"* Physical Society of London Proceedings, Section A, Vol. 62, p. 607-616, (1949).

7. R. M. Lell, *"Neutron Streaming and Anisotropic Diffusion in Partially Voided Lattices,"* Ph.D. Dissertation, The Ohio State University, (1976).

8. E. M. Gelbard and R. Lell, *"Monte Carlo Treatment of Fundamental-Mode Leakage in the Presence of Voids,"* accepted for publication Nuclear Science and Engineering.

9. P. B. Abramson, *"FX2-POOL - A Two Dimensional Coupled Hydrodynamic Thermodynamic and Neutronic Computer Model for Hypothetical Core Distruptive Accident Analysis,"* Nuclear Science and Engineering, Vol. 62, #2, p. 195 (February 1977).

10. R. B. Nicholson, Exxon Nuclear Corp, Richland Washington, personal communications, January 1977.

11. Personal conversation with Don Ferguson, December 1976.

12. Personal conversation with James Cahalan, December 1976.

13. A. A. Amsden and F. H. Harlow, *"KACHINA: An Eulerian Computer Program For Multi-Field Fluid Flows,"* Los Alamos Scientific Laboratory, LA-5680, p. 4, (1974).

14. P. M. Wood, private communication, October 5, 1976.

15. W. T. Sha, H. M. Domanus and R. C. Schmitt, *"COMMIX-Three-Dimensional, Time-Dependent, Two-Phase Flow with Non-Equilibrium Velocity and Temperature Computer Program,"* to be published in 1978.

16. W. T. Sha, H. M. Domanus, and A. A. Szewczyk, *"Development of a Computer Program for Reactor Core Thermal Hydraulics: Finite Differencing in a 3-D Staggered Mesh Suitable for Irregular Boundary Applications,"* ANL-CT-76-54 (1976).